Article

Cell Reports

Mechanisms of differential desensitization of metabotropic glutamate receptors

Graphical abstract

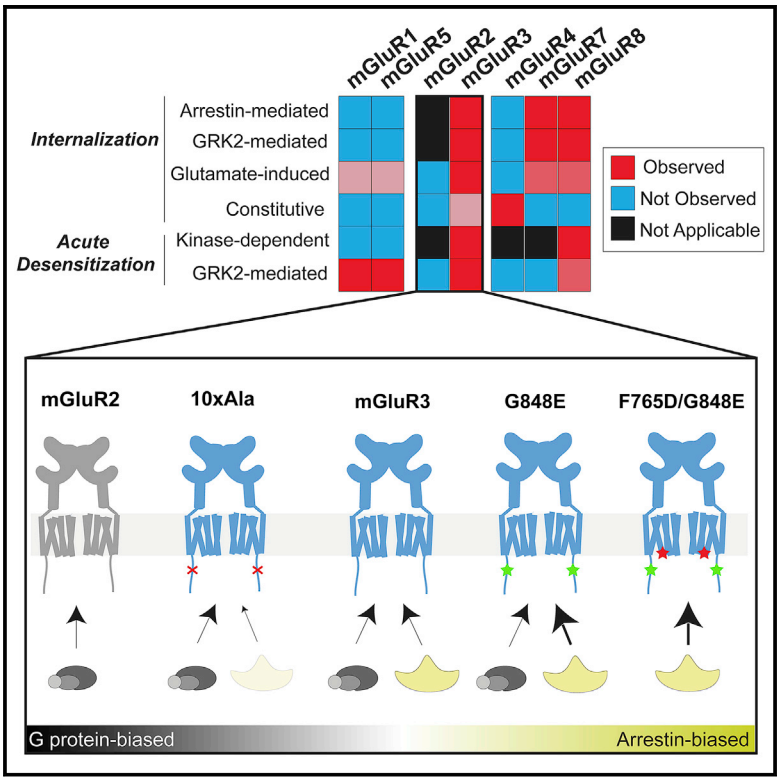

Highlights

- GRKs and arrestins mediate the fast and slow desensitization of a subset of mGluRs
- TIRF imaging reveals scaffold and catalytic coupling between mGluR3 and β-arrestins
- Different patterns of Ser and Thr control the desensitization of group II mGluRs
- Mutational analysis reveals G protein- and β-arrestin-biased mGluR3 variants

Authors

Nohely Abreu, Amanda Acosta-Ruiz, Guoqing Xiang, Joshua Levitz

Correspondence

jtl2003@med.cornell.edu

In brief

Abreu et al. use high-resolution imaging and electrophysiology to reveal distinct desensitization properties across subtypes of the metabotropic glutamate receptor (mGluR) family. Comparative analysis of group II mGluR subtypes identifies a Ser/Thr-rich region in the C-terminal domain of mGluR3 that mediates both rapid GRK-mediated desensitization and arrestin-mediated internalization.

Abreu et al., 2021, Cell Reports *35*, 109050
April 27, 2021
https://doi.org/10.1016/j.celrep.2021.109050

CellPress

Cell Reports

CellPress
OPEN ACCESS

Article

Mechanisms of differential desensitization of metabotropic glutamate receptors

Nohely Abreu,[1,2] Amanda Acosta-Ruiz,[1,2,3] Guoqing Xiang,[2,3] and Joshua Levitz[1,2,4,*]
[1]Biochemistry, Cell and Molecular Biology Graduate Program, Weill Cornell Medicine, New York, NY, USA
[2]Department of Biochemistry, Weill Cornell Medicine, New York, NY, USA
[3]These authors contributed equally
[4]Lead contact
*Correspondence: jtl2003@med.cornell.edu
https://doi.org/10.1016/j.celrep.2021.109050

SUMMARY

G protein-coupled receptors (GPCRs) interact with intracellular transducers to control both signal initiation and desensitization, but the distinct mechanisms that control the regulation of different GPCR subtypes are unclear. Here we use fluorescence imaging and electrophysiology to examine the metabotropic glutamate receptor (mGluR) family. We find distinct properties across subtypes in both rapid desensitization and internalization, with striking differences between the group II mGluRs. mGluR3, but not mGluR2, undergoes glutamate-dependent rapid desensitization, internalization, trafficking, and recycling. We map differences between mGluRs to variable Ser/Thr-rich sequences in the C-terminal domain (CTD) that control interaction with both GPCR kinases and β-arrestins. Finally, we identify a cancer-associated mutation, G848E, within the mGluR3 CTD that enhances β-arrestin coupling and internalization, enabling an analysis of mGluR3 β-arrestin-coupling properties and revealing biased variants. Together, this work provides a framework for understanding the distinct regulation and functional roles of mGluR subtypes.

INTRODUCTION

G protein-coupled receptors (GPCRs) sense diverse extracellular signals to initiate intracellular responses. The temporal properties of GPCR signaling are regulated by desensitization, a process that involves both uncoupling of the receptor from G proteins via steric blockage and receptor internalization. Generally, GPCR kinases (GRKs) and arrestins regulate GPCR desensitization, although GRK- and arrestin-independent mechanisms also exist (Ferguson et al., 1996; Gainetdinov et al., 2004; Ménard et al., 1997; Rajagopal and Shenoy, 2018). Canonically, GRKs are recruited to activated GPCRs and either compete with G proteins for receptor access or directly bind G proteins to contribute to rapid desensitization (Lodowski et al., 2003; Tesmer et al., 2005). GRKs can also phosphorylate the cytosolic C-terminal domain (CTD) of the receptor to enable the recruitment of β-arrestin (β-arr) 1 or β-arr2. β-arr serves as a scaffold for the recruitment of either endocytic proteins (e.g., clathrin) or signaling proteins (e.g., ERK) (Hilger et al., 2018; Peterson and Luttrell, 2017; Shenoy and Lefkowitz, 2011). This desensitization framework has been established through the study of prototypical GPCRs, but different GPCR subtypes use distinct sets of mechanisms that are only partially deciphered.

Although a structural understanding of GPCR/GRK interaction is limited (Komolov and Benovic, 2018), structural and biophysical studies have revealed complexity in the interactions between β-arr and receptors. This includes modes of interactions in which β-arr binds the CTD, the transmembrane core, or both domains of the receptor (Cahill et al., 2017; Kang et al., 2015; Kumari et al., 2016; Shukla et al., 2014; Staus et al., 2020) and associated conformational dynamics within both β-arr subtypes (Latorraca et al., 2018; Lee et al., 2016; Nuber et al., 2016). Many GPCRs have been shown to couple to β-arr, but the nature of this interaction depends on the receptor subtype, the β-arr subtype, and the receptor ligand used. Key determinants of β-arr-coupling propensity are the degree and the pattern of receptor phosphorylation (Miess et al., 2018; Nobles et al., 2011; Sente et al., 2018), leading to the proposal of phosphorylation codes (phospho-codes) that are recognized by β-arr (Zhou et al., 2017). GPCRs are broadly characterized into class A and class B based on the nature of their β-arr coupling (Kohout et al., 2001; Oakley et al., 2000). In the strong interactions of class B GPCRs, such as the V2 vasopressin receptor, β-arr internalizes with the receptor, which can lead to slow recycling and degradation (DeWire et al., 2007). In the weaker interactions of class A GPCRs, such as the beta-2 adrenergic receptor (β_2AR), receptor/β-arr complexes do not typically persist into the endosome and receptors are recycled relatively quickly compared with class B GPCRs. Recently, it was shown that some GPCRs can engage in transient interactions with β-arr to produce non-stoichiometric catalytic activation and accumulation of β-arr in clathrin-coated structures (Eichel et al., 2016, 2018). The complexity of β-arr coupling suggests that GRK coupling may be similarly complex, motivating a thorough analysis of transducer coupling across receptor subtypes.

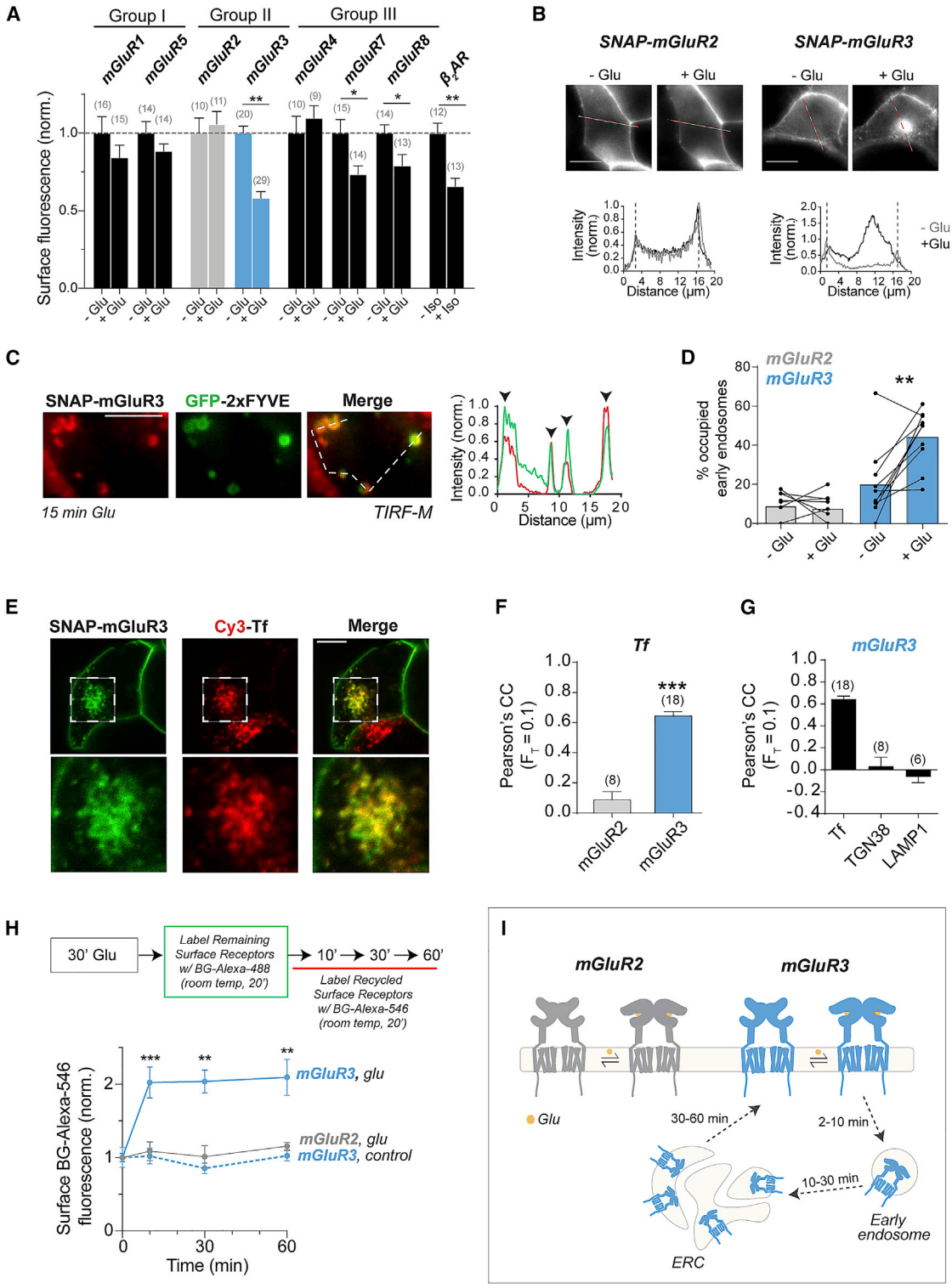

Figure 1. Glutamate-dependent internalization of mGluRs

(A) Surface fluorescence from HEK293T cells expressing either SNAP-tagged mGluRs or β_2AR with and without 60 min agonist stimulation (1–10 mM Glu and 10 μM Iso) before BG-Alexa 546 labeling. Values were normalized to the fluorescence of a given receptor without an agonist. Unpaired t tests, ***p < 0.0001 for mGluR3, *p = 0.02 for mGluR7, *p = 0.03 for mGluR8, and ***p = 0.0004 for β_2AR.

(legend continued on next page)

In contrast to family A and B GPCRs, which form the basis of existing desensitization models, the desensitization of family C GPCRs is less understood (Ellaithy et al., 2020). In particular, there is a lack of consensus regarding desensitization for metabotropic glutamate receptors (mGluRs) (Iacovelli et al., 2013; Suh et al., 2018), and comparative analysis across subtypes is lacking. Among the well-studied group I mGluRs (mGluR1 and mGluR5), evidence exists for constitutive clathrin-independent internalization (Fourgeaud et al., 2003; Francesconi et al., 2009), and control of receptor surface levels via kinases and accessory proteins have been observed (Suh et al., 2018). Evidence for interactions between mGluRs and GRKs or β-arr is limited and indirect (Emery et al., 2010; Mundell et al., 2001; Stoppel et al., 2017), leaving mechanistic details unknown.

The group II mGluRs (mGluR2 and mGluR3) are ubiquitous throughout the nervous system, where they couple to $G_{i/o}$-family G proteins to play roles in neuromodulation and are drug targets for neurological and psychiatric disorders (Nicoletti et al., 2011; Reiner and Levitz, 2018). mGluR3 is also expressed in the skin, where it has been linked to melanoma (Neto and Ceol, 2018; O'Hayre et al., 2013; Prickett et al., 2011). Like most family C GPCRs, mGluR2 and mGluR3 have large extracellular ligand binding domains (LBDs), 7-helix transmembrane domains (TMDs), and relatively short (~50 aa) intracellular CTDs (Ellaithy et al., 2020). Although the highly homologous (~70% sequence identity) mGluR2 and mGluR3 have been treated as a single entity, biophysical studies have shown that they have distinct activation properties, with mGluR3 showing ~10-fold higher apparent glutamate affinity and more basal activation (Tora et al., 2018; Vafabakhsh et al., 2015). This suggests that these receptors have unique physiological profiles, raising the question of their desensitization and signaling dynamics. A previous study used an endpoint cyclic AMP assay to suggest that mGluR2, but not mGluR3, is resistant to GRK- and β-arr-mediated desensitization (Iacovelli et al., 2009), but otherwise little is known about group II mGluR desensitization.

In this study, we elucidate the molecular mechanisms of mGluR desensitization using fluorescence imaging and functional assays. Among the group II mGluRs, we find that mGluR3, but not mGluR2, is subject to extensive glutamate-dependent internalization via GRK and β-arr. Compared with mGluR3, group I and group III mGluRs show distinct properties, including β-arr-independent glutamate-induced (mGluR1 and mGluR5) and constitutive (mGluR4) internalization. A subset of mGluRs (mGluR1, mGluR3, mGluR5, and mGluR8) shows GRK-mediated functional desensitization on the timescale of seconds. After characterizing GRK and β-arr sensitivity across subtypes, we focus on deciphering the β-arr-coupling dynamics of mGluR3 and probing the mechanistic basis of the differences between group II mGluRs. Altogether, our results indicate that different mGluRs have fundamentally different signaling properties and provide insight into the mechanisms of GRK and β-arr coupling of family C GPCRs.

RESULTS

Glutamate-dependent internalization and trafficking of mGluRs

We first asked whether mGluRs undergo internalization following activation by labeling N-terminal SNAP-tagged mGluRs with the membrane impermeable BG-Alexa 546 fluorophore in HEK293T cells and measuring the loss of surface receptor fluorescence following agonist incubation. Saturating glutamate led to a ~40% reduction in surface fluorescence for mGluR3 (Figure 1A; Figure S1A). A similar agonist-induced decrease in surface levels was observed for β_2AR (Figure 1A; Figure S1A), a prototypical family A GPCR known to undergo agonist-induced internalization (von Zastrow and Kobilka, 1992). The group III mGluRs, mGluR7 and mGluR8, also showed a clear but smaller (~25%) reduction in surface levels, and the group I mGluRs, mGluR1 and mGluR5, showed a small (~10%) decrease (Figure 1A). Strikingly, surface levels of both mGluR2 (group II) and mGluR4 (group III) showed no sensitivity to glutamate treatment. Altogether, these results motivated a comparative analysis of the closely related group II mGluRs, mGluR2 and mGluR3, which showed different extents of internalization.

We next imaged cells expressing receptors labeled with BG-Alexa 546 before glutamate treatment. Although mGluR2 remained on the surface, mGluR3 showed an increase in intracellular fluorescence (Figure 1B; Figure S1B), similar to β_2AR (Figure S1C). Some accumulation of mGluR3 was also seen in the absence of glutamate addition (Figure S1D), likely because of its basal activity (Vafabakhsh et al., 2015) and the release of glutamate from HEK293T cells (Tora et al., 2018). About 60% of glutamate-treated cells showed mGluR3 internalization versus <10% of cells showing negligible levels of mGluR2 internalization

(B) Images of cells expressing SNAP-mGluR2 (left) or SNAP-mGluR3 (right) before and after 30 min 1 mM Glu treatment with intensity line scans (bottom). Dotted lines denote the plasma membrane location.
(C) TIRF image (left) and line scan (right) showing colocalization of SNAP-mGluR3 (red) and GFP-2xFYVE (green) following Glu treatment.
(D) Quantification of the percentage of GFP-2xFYVE puncta that show colocalization with SNAP-mGluR2 or SNAP-mGluR3 before and after 15 min of Glu application. Lines connect values for individual cells, and bars show average values. Paired t test, **p = 0.004.
(E) Confocal images showing colocalization of SNAP-mGluR3 and Cy3-transferrin (Cy3-Tf) following 30 min treatment with 1 mM Glu.
(F) Pearson's correlation coefficient (PCC) comparing the top 10% of pixels between mGluR2 or mGluR3 with Cy3-Tf following incubation in 1 mM Glu for 30 min. Unpaired t test, ***p < 0.0001.
(G) Quantification of PCC comparing colocalization of mGluR3 and Cy3-Tf, mCh-TGN38, or LAMP1-YFP following incubation in 1 mM Glu for 30 min.
(H) Top, schematic describing a recycling experiment in which receptors are internalized with Glu, remaining surface receptors are labeled with BG-Alexa 488, and subsequent labeling with BG-Alexa 546 is indicative of recycled receptors. For the control (blue dotted line), no Glu treatment was given. Unpaired t tests, ***p = 0.0002 for 10 min, ***p = 0.0002 for 30 min, and ***p = 0.0003 for 60 min.
(I) Schematic summarizing major results. mGluR2 remains on the surface following activation, whereas mGluR3 internalizes into early endosomes, traffics to the ERC, and recycles back to the surface.
Error bars show SEM. Scale bar, 10 μm (B and E) or 5 μm (C). Number of cells tested (F and G) or fields of cells analyzed (A) is in parentheses.

(Figure S1E). Treating cells with an mGluR3-negative allosteric modulator (ML289) or competitive antagonist (LY341495) decreased mGluR3 internalization (Figure S1E), confirming the requirement of receptor activation. Importantly, an EC_{50} level (1 μM) of glutamate (Figure S1F) or 5 min of glutamate stimulation was sufficient to internalize mGluR3 (Figure S1G). Similar results, in which mGluR3, but not mGluR2, showed internalization, were observed in HEK293 cells (Figure S1H).

We also imaged HEK293T cells to test internalization of group I and III mGluRs, and results agreed with the surface labeling assay (Figure S1I). mGluR7 and mGluR8 showed modest, glutamate-induced intracellular fluorescence, whereas limited intracellular puncta were observed for mGluR1 and mGluR5. Unexpectedly, mGluR4 showed intracellular puncta in the presence and absence of glutamate. Treatment with a saturating concentration of LY341495 did not alter mGluR4 internalization (Figure S1J), confirming that it is constitutive and glutamate independent. This result shows that despite both mGluR2 and mGluR4 showing no net glutamate-induced internalization (Figure 1A), they have distinct behavior.

We next characterized the trafficking of mGluR3 following internalization. Using total internal reflection fluorescence (TIRF) microscopy, we observed an increase in cytosolic fluorescent puncta for mGluR3, but not mGluR2, within 5 min of glutamate treatment (Figure S2B). A sparse population of fluorescent puncta was observed for all other mGluRs (Figure S2A). mGluR3 puncta showed glutamate-dependent colocalization with GFP-2xFYVE (Gillooly et al., 2000), indicating that puncta represent internalized receptors within early endosomes (Figures 1C and 1D; Figure S2C).

Following internalization into endosomes, GPCRs can traffic to lysosomes for degradation (Marchese and Benovic, 2001; Shenoy et al., 2001), the trans-Golgi network (TGN) for sorting (Abdullah et al., 2016), or the endocytic recycling compartment (ERC) (von Zastrow and Kobilka, 1992). We tested whether mGluR3 accumulates in the ERC using transferrin (Tf) as a marker (Maxfield and McGraw, 2004). Confocal microscopy revealed that mGluR3, but not mGluR2, colocalizes with internalized Cy3-Tf after glutamate treatment (Figures 1E and 1F; Figure S2D). In contrast, minimal colocalization of mGluR3 was observed with TGN and lysosome markers (Figure 1G; Figures S2E and S2F). Trafficking to the ERC suggests that mGluR3 recycles to the surface following internalization, which we confirmed by measuring the return of surface mGluR3 following glutamate incubation using a modified version of the surface labeling assay (Figure 1H; Figure S2G). We conclude that mGluR2 remains on the surface following activation, whereas mGluR3 internalizes, traffics to the ERC, and traffics back to the surface within 1 h (Figure 1I).

GRKs and β-arrestins mediate the internalization of a subset of mGluRs

The canonical pathway of GPCR endocytosis requires β-arr binding followed by targeting to clathrin-coated pits (CCPs). However, there is evidence that family C GPCRs, including group I mGluRs, internalize via β-arr and clathrin-independent mechanisms (Fourgeaud et al., 2003; Francesconi et al., 2009). Therefore, we decided to test which transducers mediate mGluR internalization.

To test whether G protein coupling is required for mGluR3 internalization, we transfected cells with pertussis toxin (PTX) (Mangmool and Kurose, 2011), which abolished the ability to activate G protein-coupled inward rectifier potassium (GIRK) channels in a patch-clamp assay (Figure S3A). Glutamate-induced mGluR3 internalization was slightly enhanced with PTX expression (Figures 2A and 2B; Figure S3B), indicating that G proteins do not drive mGluR3 internalization and may compete with other transducers. In contrast, treatment with the GRK2/3 inhibitor, compound 101 (cmpd101), or coexpression of a dominant-negative (DN) β-arr1 (Lin et al., 1997), greatly reduced mGluR3 internalization (Figures 2A and 2B; Figure S3B). Moreover, GRK2 or β-arr expression increased internalization of mGluR3, but not mGluR2 (Figures 2C and 2D; Figure S3B). mGluR3 internalization depended on the GRK2 kinase domain, because overexpressing a kinase-dead mutant (K220R) (Kong et al., 1994) exhibited a dominant-negative effect (Figures S3C and S3D). In contrast, a GRK2 mutant that is unable to bind $G_{\beta\gamma}$ (GRK2-R587Q) (Carman et al., 2000) could still enhance internalization (Figures S3C and S3D).

We next asked whether internalization of other mGluR subtypes depends on GRK and β-arr. GRK2 expression enhanced internalization of mGluR7 and mGluR8 (Figure 2E) but did not affect internalization of mGluR1 and mGluR5 (Figure 2E) or mGluR4 (Figure S3E). Next, we tested arrestin dependence by using β-arr double-knockout (DKO) cells (Luttrell et al., 2018), which showed dramatically reduced mGluR3 internalization (Figure 2F; Figure S3F). Similarly, mGluR7 and mGluR8 showed reduced internalization in DKO cells, whereas the internalization of mGluR1 and mGluR5 was not altered (Figure 2F; Figure S3G). Basal internalization of mGluR4 was maintained in β-arr DKO cells, suggesting that its constitutive internalization proceeds through a β-arr-independent mechanism (Figure S3G). These data show that internalization of mGluR3, mGluR7, and mGluR8 depend on β-arr and GRK.

GRKs mediate rapid desensitization of mGluRs

Given that internalization of a subset of mGluRs depends on GRKs and β-arr (Figure 2), we asked whether these transducers also produce rapid functional desensitization using GIRK currents as a readout. GIRK channels are activated by binding of $G_{\beta\gamma}$ proteins (Logothetis et al., 1987; Whorton and MacKinnon, 2013) and are major native effectors of $G_{i/o}$-coupled GPCRs, including group II/III mGluRs (Dutar et al., 1999; Saugstad et al., 1996). mGluR2-mediated GIRK currents showed minimal desensitization, but mGluR3-mediated currents showed pronounced desensitization (Figures 3A–3C). Consistent with this, following 3 consecutive applications of glutamate, the peak amplitudes of mGluR2-mediated currents were maintained, whereas mGluR3-mediated currents progressively decreased (Figures S4A–S4C). Despite higher surface expression levels of mGluR2 under our conditions (Figure S4D), mGluR3 activation led to substantially smaller current amplitudes (Figure S4E). This suggests that a population of desensitized surface mGluR3 is unable to signal.

We next asked how different transducers contribute to mGluR3 desensitization. Raveh et al. (2010) identified a

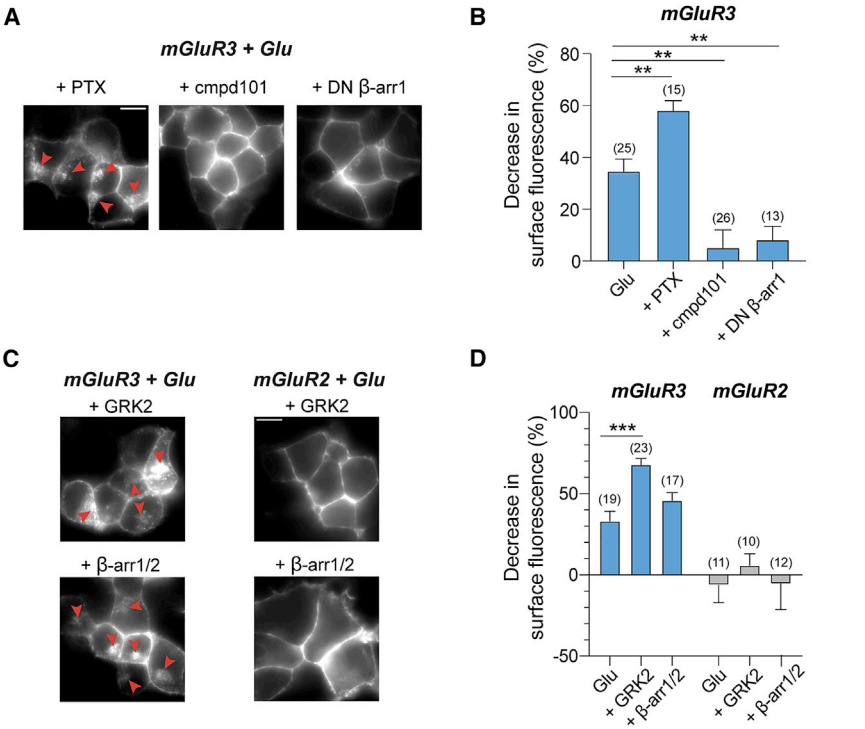

Figure 2. GRK and β-arrestin dependence of mGluR internalization

(A and B) DN β-arr1 (S412D) and cmpd101 reduce internalization of mGluR3, whereas PTX enhances internalization, as seen in representative images (A) and quantification of surface fluorescence reduction following Glu application (B). Red arrows denote internalized receptors. Unpaired t tests, **p = 0.001 for PTX, **p = 0.001 for cmpd101, and **p = 0.001 for DN β-arr1.

(C and D) Overexpression of GRK2 or β-arr enhances internalization of mGluR3, but not mGluR2. Unpaired t test, ***p < 0.0001 for GRK2.

(E) Overexpression of GRK2 enhances internalization of mGluR7 and mGluR8, but not mGluR1 or mGluR5. Unpaired t tests, ***p = 0.0003 for mGluR3, **p = 0.004 for mGluR7, and **p = 0.006 for mGluR8.

(F) SNAP-mGluRs were expressed in a CRISPR β-arr DKO HEK293 cell line. Internalization for mGluRs in β-arr DKO cells compared with the parental cell line using quantification of surface fluorescence reduction following Glu application. Unpaired t tests, ***p < 0.0001 for mGluR3, *p = 0.02 for mGluR7, and *p = 0.04 for mGluR8.

Number of fields of cells analyzed is in parentheses. Error bars show SEM. Scale bar, 10 μm.

mechanism whereby GRKs bind $G_{\beta\gamma}$ proteins to desensitize GIRK currents following activation of the adenosine-1 receptor (A1R). mGluR2 and the M4 muscarinic acetylcholine receptor were not sensitive to GRKs, although no mechanism for this subtype specificity was identified. Here we focused on the GRK2 subtype, which is expressed throughout the nervous system (Erdtmann-Vourliotis et al., 2001) and in HEK293T cells (Violin et al., 2006). As previously reported (Raveh et al., 2010), GRK2 overexpression had no effect on the desensitization of mGluR2-mediated GIRK currents (Figure 3D). However, for mGluR3, GRK2 dose-dependently increased the magnitude and speed of desensitization (Figures 3E and 3F; Figures S4F and S4L). GRK2 expression also led to a large reduction in the amplitude of mGluR3-induced currents (Figure S4G), whereas a small (~25%) decrease of mGluR2-induced current amplitude was seen (Figure S4G). Importantly, no relationship between current amplitude and desensitization kinetics was observed, indicating that the enhanced desensitization produced by GRK2 is not a consequence of reduced mGluR3 surface expression (Figure S4H).

Next, we probed the mechanism of GRK2-mediated desensitization by first testing the role of GRK2-$G_{\beta\gamma}$ binding. We coexpressed GRK2-R587Q (Carman et al., 2000) and found that it was unable to increase mGluR3 desensitization (Figure 3F; Figures S4I–S4K). We also tested kinase-dead GRK2-K220R (Kong et al., 1994), and in contrast to what was reported for the A1R (Raveh et al., 2010), it did not produce an effect on the desensitization of mGluR3-mediated currents, despite similar expression to wild-type (WT) GRK2 (Figure 3F; Figures S4I–S4K). The need for a catalytically active GRK2 raised the possibility that β-arr recruitment contributes to rapid desensitization. However, overexpression of β-arr1 and β-arr2 did not affect desensitization (Figure 3F; Figure S4K). Altogether, these results demonstrate that both functional kinase and $G_{\beta\gamma}$ binding domains of GRK2 mediate rapid and specific mGluR3 desensitization (Figure 3G). The ability of mGluR3, but not mGluR2, to be desensitized by GRK2 despite both receptors producing free $G_{\beta\gamma}$ argues that GRK2 is recruited directly to the receptor rather than to free G proteins (Figure 3G; Figure S3D).

Group III mGluRs also showed variable propensities for internalization (Figure 2F). Consistent with its sensitivity to GRK2 in internalization assays (Figure 2E), mGluR8 showed modest but clear enhancement of desensitization following GRK2 coexpression (Figures 3H and 3I; Figure S4L). Similar to mGluR3, the K220R mutation prevented GRK2-mediated desensitization of

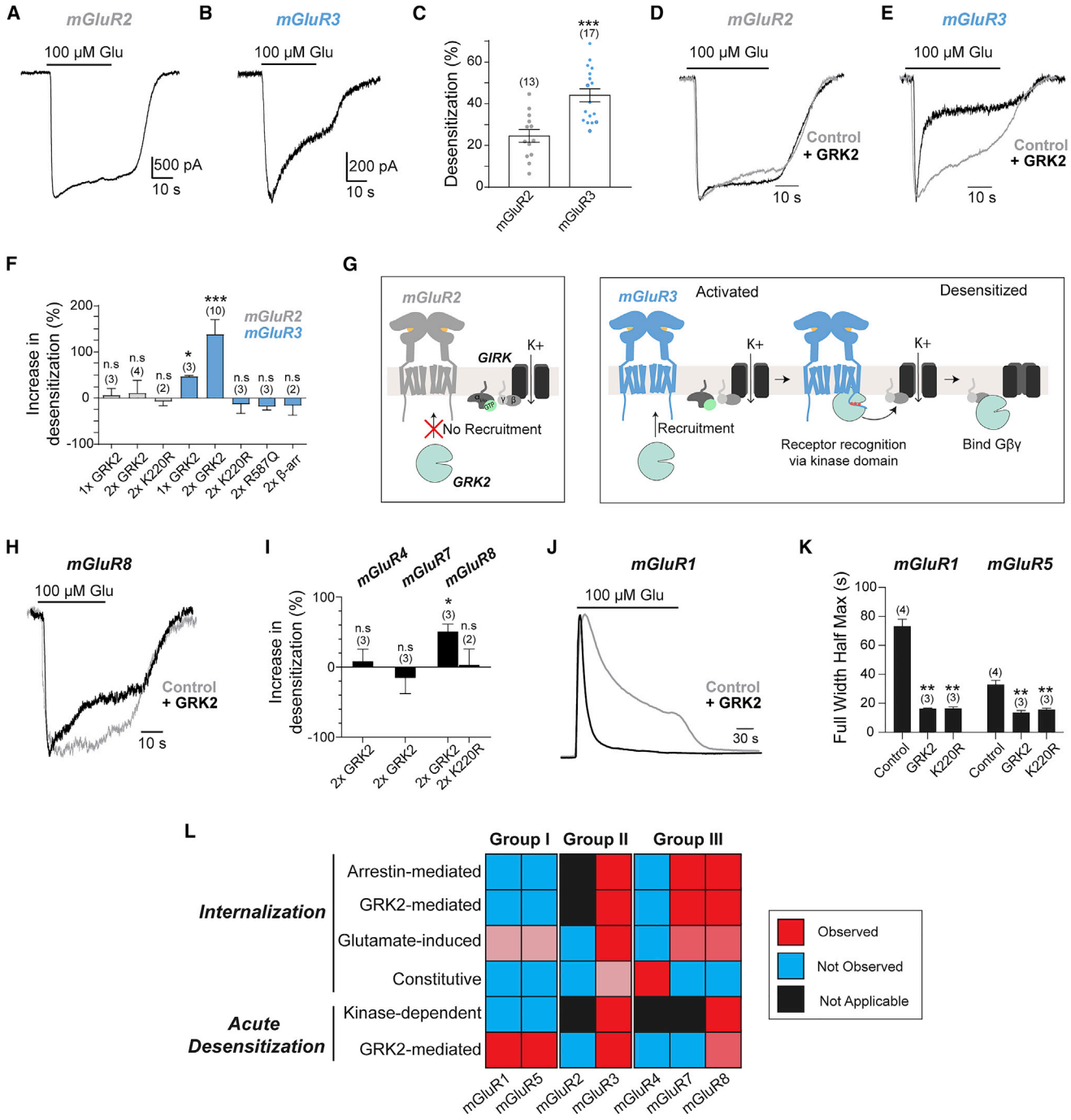

Figure 3. GRK2-mediated rapid desensitization of mGluRs

(A and B) Representative whole-cell patch-clamp recordings from HEK293T cell expressing SNAP-mGluR2 (A) or SNAP-mGluR3 (B) showing an inward GIRK current induced by Glu application.

(C) Quantification of the percentage of desensitization of GIRK currents showing larger desensitization of mGluR3 responses. Unpaired t test, ***$p < 0.0001$.

(D and E) Recordings showing sensitivity of GIRK currents induced by mGluR2 (D) or mGluR3 (E) with and without GRK2 overexpression.

(F) Summary bar graph showing the percentage increase in desensitization on mGluR2- and mGluR3-mediated GIRK currents with overexpression of GRK2, GRK2 mutants, or β-arr. Unpaired t test versus mGluR3 control, *$p = 0.04$ for 1xGRK2 and ***$p < 0.0001$ for 2xGRK2.

(G) Schematic showing differential GRK recruitment and rapid desensitization for mGluR2 (left) and mGluR3 (right).

(H) Recordings showing modest desensitization of mGluR8-mediated GIRK currents with and without GRK2 overexpression over 30 s Glu application.

(I) Summary bar graph showing the percentage increase in desensitization of mGluR4-, mGluR7-, and mGluR8-mediated GIRK currents with overexpression of WT GRK2 or K220R. Unpaired t test of mGluR8 control versus mGluR8 + GRK, *$p = 0.03$.

(legend continued on next page)

GIRK currents by mGluR8 (Figure 3I). Surprisingly, mGluR7-mediated currents did not exhibit enhanced desensitization with GRK2 overexpression (Figure 3I; Figures S4M and S4O). Slower ON-kinetics of mGluR7 currents (~5–10 versus ~1–3 s) may prevent the resolution of fast desensitization components. Consistent with its resistance to GRK- and β-arr-mediated internalization (Figure 2), mGluR4 did not show GRK2-mediated functional desensitization (Figure 3I; Figures S4N and S4O). However, current amplitudes were decreased for all three group III mGluRs tested (Figure S4P), which may indicate sensitivity over longer timescales.

We also examined the GRK2 sensitivity of the Gq-coupled group I mGluRs using the fluorescent calcium sensor R-GECO (Zhao et al., 2011). The duration and rate of decay, but not the amplitude, of glutamate-induced calcium transients were dramatically reduced with expression of GRK2 for both mGluR1 and mGluR5 (Figures 3J and 3K; Figures S4Q–S4S). Furthermore, extended mGluR5 activation produces oscillatory calcium signals (Kawabata et al., 1996). GRK2 expression reduced the percentage of cells producing oscillatory responses, leading to many cells that showed a single calcium transient (Figures S4T and S4U). Unlike group II and III mGluRs, GRK2-mediated desensitization of group I mGluRs did not depend on a functional kinase domain based on the strong effect of GRK2-K220R (Figure 3K; Figures S4S and S4U).

Altogether, these results show that variable propensities for and modes of desensitization and internalization are seen throughout the mGluR family (Figure 3L), which can shape the signaling properties of each subtype.

Mechanistic analysis of group II mGluRs: Coupling of β-arrestins to mGluR3

We next focused on deciphering the mechanisms of differential transducer coupling of the group II subfamily. To measure surface translocation of cytosolic β-arr, we coexpressed either β-arr1-YFP or β-arr2-YFP with mGluR3 or mGluR2 and observed β-arr surface recruitment only with mGluR3 activation (Figure 4A). As expected, β-arr recruitment was insensitive to PTX but was blocked by mGluR3 antagonists (Figures S5A and S5B). Similar levels of recruitment of β-arr1 or β-arr2 indicates that mGluR3 has no major β-arr subtype preference, unlike the preference for β-arr2 seen with the β_2AR (Figures S5C and S5D) (Kohout et al., 2001; Oakley et al., 2000).

We characterized the timing and stability of mGluR3/β-arr complexes by simultaneously imaging mGluR3 and β-arr-YFP. We observed surface recruitment of β-arr1 or β-arr2 by mGluR3 within 3 min, with further accumulation until ~10 min after glutamate application (Figure 4B; Figure S5E). After 10 min, β-arr remained on the surface as mGluR3 internalized, indicating that β-arr does not cotraffic into the ERC (Figure 4B; Figure S5E). β-arr translocation was not detectable following activation of mGluR2 at any time point (Figure S5F), but the β_2AR produced a fluorescence distribution similar to that of mGluR3 (Figure S5G). Consistent with this, minimal colocalization of β-arr2-RFP and GFP-2xFYVE was observed following mGluR3 activation (Figures S5H and S5I), although the level of colocalization was slightly higher with β_2AR activation compared with mGluR3 (Figure S5I).

To further characterize the coupling of group II mGluRs and β-arr at the cell surface, we simultaneously imaged receptors and β-arr using TIRF microscopy. Following 10–15 min of glutamate application, no features were observed in mGluR2-expressing cells (Figure 4C; Figure S5J), but we observed bright puncta for both β-arr and mGluR3 (Figure 4D; Figure S5K). Although β-arr puncta were largely immobile, receptor puncta showed a mix of immobile and mobile spots (Videos S1 and S2). Similar puncta formed with β_2AR and β-arr2, consistent with previous reports (Eichel et al., 2016, 2018) (Figure 4E). Quantification of puncta density revealed higher levels of both receptor and β-arr2 puncta for β_2AR than mGluR3, with few puncta in mGluR2-expressing cells (Figure 4F; Figure S5L). In mGluR3-expressing cells, ~40% fewer receptor puncta were observed compared with β-arr2 puncta (Figure 4F; Figure S5L). In contrast, similar densities of receptor and β-arr2 puncta were observed for β_2AR (Figure 4F). This discrepancy in puncta densities suggests that one mGluR3 can activate multiple β-arr molecules, as was reported for the beta-1 adrenergic receptor (β_1AR) (Eichel et al., 2018). In line with this, some puncta were detected under basal conditions (Figure S5M) but with a nearly 3:1 ratio of β-arr to receptor puncta (Figure 4F; Figure S5L). This supports the notion of catalytic coupling and suggests that a low level of receptor activation leads to a transient form of coupling, whereas stronger agonism may enhance stability. Line scans revealed colocalization between receptor and β-arr, although the degree of colocalization was lower for mGluR3 than for β_2AR (Figures 4D, 4E, and 4G).

We characterized the process of mGluR3/β-arr coupling by imaging CCPs and observed strong colocalization between β-arr and CLC-mCh puncta in mGluR3- or β_2AR-expressing cells (Figure 4H; Figures S5M–S5O). Furthermore, in contrast to the mobility of GFP-2xFYVE-positive early endosomes (Video S3) most CLC-mCh-positive CCPs appear to be immobile (Video S4). This suggests that the immobile population of receptors occurs in CCPs with immobile β-arr clusters and the mobile receptors are likely in early endosomes.

Altogether, our data show interaction between mGluR3 and both β-arr and indicate that formation of this complex is critical for recruitment of mGluR3 to CCPs and receptor internalization.

(J) Average trace representing calcium transients produced by ~50 cells expressing only mGluR1 or with GRK2 overexpression.
(K) Summary bar graph showing the full duration at half-maximum of calcium transients mediated by mGluR1 and the first calcium transient mediated by mGluR5 activation, without and with overexpression of WT GRK2 or K220R. ** indicates statistical significance. Unpaired t tests, p = 0.002 for mGluR1 control versus GRK2, p = 0.001 for mGluR1 control versus K220R, p = 0.005 for mGluR5 control versus GRK2, and p = 0.009 for mGluR5 control versus K220R. Number of cells analyzed are as follows: n = 142 for mGluR1 control, 134 for GRK2, and 149 for K220R; n = 287 for mGluR5 control, 126 for GRK2, and 88 for K220R.
(L) Summary heatmap showing the relative propensities for acute desensitization and internalization across mGluRs, and their dependence on interactions with β-arr and GRK2.
Error bars show SEM. Number of cells recorded from (A) or independent experiments (F, I, and K) is in parentheses.

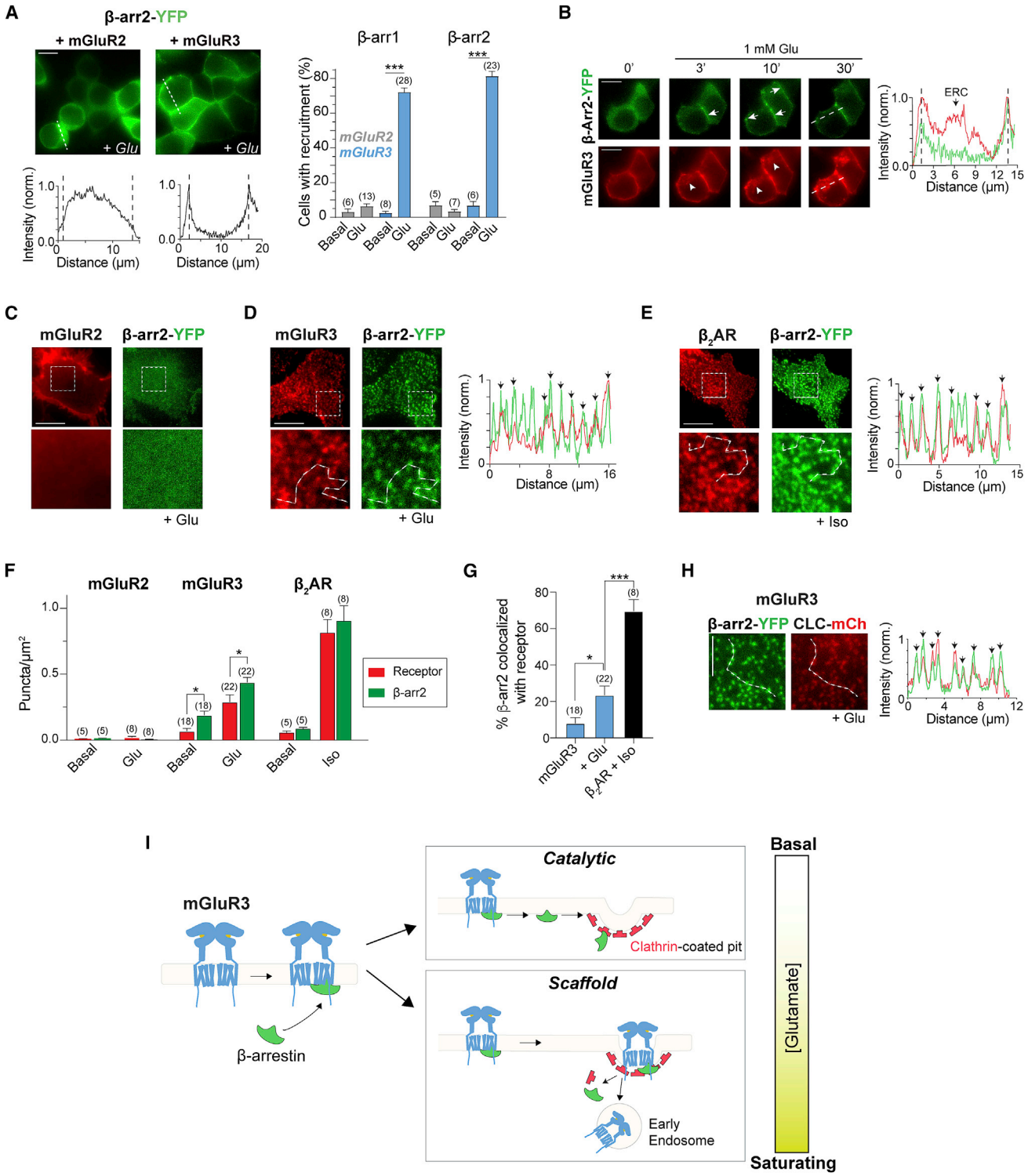

Figure 4. mGluR3 recruits β-arrestins via scaffold and catalytic coupling

(A) Left, representative images and intensity line scans showing Glu-dependent surface recruitment of β-arr2 by mGluR3. Right, quantification of the percentage of cells that exhibit β-arr surface recruitment. Unpaired t tests for mGluR3, ***$p < 0.0001$ for β-arr1 and ***$p < 0.0001$ for β-arr2.

(B) Time-lapse images showing Glu-dependent surface recruitment of β-arr2 and subsequent internalization of only mGluR3. Arrows point at β-arr2 accumulation on the cell surface. Arrowheads denote internalized receptors.

(legend continued on next page)

In addition, our data suggest that mGluR3 shows a mix of transient coupling that leads to independent clusters of activated β-arr (i.e., catalytic coupling) and colocalized mGluR3/β-arr complexes that persist into CCPs, but not endosomes (i.e., scaffold coupling) (Figure 4I).

A Ser/Thr-rich subregion of the mGluR3 CTD controls internalization and rapid desensitization

Having observed GRK- and β-arr-dependent desensitization of mGluR3, but not mGluR2, we aimed to identify the molecular determinants of the differences between receptors with a focus on the CTD. Removing the CTD of mGluR3 (mGluR3-ΔCTD) substantially reduced internalization (Figures 5A and 5B), although the degree of internalization for mGluR3-ΔCTD was still above the background levels seen with mGluR2. We next swapped the CTDs of mGluR2 and mGluR3 and observed a clear effect on each subtype. mGluR3-mGluR2CTD showed no internalization, whereas mGluR2-mGluR3CTD exhibited internalization (Figures 5A and 5B), demonstrating that the CTD is the major determinant of group II mGluR desensitization. Surprisingly, mGluR3-mGluR2CTD exhibited even less internalization than mGluR3-ΔCTD, suggesting that the mGluR2 CTD may serve an inhibitory role (Figures 5A and 5B). Consistent with this, removing the CTD from mGluR2 (mGluR2-ΔCTD) resulted in a small increase in internalization (Figures 5A and 5B). We tested the aforementioned CTD perturbations in the surface labeling assay and found that only WT mGluR3 and mGluR2-mGluR3CTD showed reductions of surface receptor levels following glutamate treatment (Figure 5C). This is in line with cell imaging, because the weak internalization of mGluR3-ΔCTD and mGluR2-ΔCTD (Figures 5A and 5B) is unlikely to produce a measurable change in the total level of surface receptors. For each CTD chimera, we also tested the ability to recruit β-arr following glutamate application under expression-matched conditions (Figure S6A) and found consistent results in which swapping mGluR CTDs swapped the ability to recruit β-arr (Figures S6B–S6D).

We also asked whether the CTDs control the differences in rapid desensitization between mGluR2 and mGluR3. The traditional view is that the CTD is not involved in the GRK-mediated rapid uncoupling of GPCRs from G proteins. However, GIRK currents induced by mGluR3-mGluR2CTD showed no sensitivity to GRK2 expression, whereas currents induced by mGluR2-mGluR3CTD showed enhanced desensitization (Figures 5D–5F; Figures S6F and S6G). To confirm the importance of the CTD to rapid GRK-mediated desensitization, we tested mGluR3-ΔCTD, which showed no change in desensitization with GRK2 (Figures S6E and S6F). GRK2 decreased amplitudes mediated by both mGluR3-ΔCTD and mGluR2-mGluR3CTD, but not mGluR3-mGluR2CTD (Figure S6H).

Having identified the CTD as the major mediator of differential mGluR desensitization, we sought to identify critical CTD subregions. Sequence alignment revealed a stretch of residues in mGluR2 and mGluR3 that contains a high density of Ser and Thr, which we termed the ST-rich region (Figure 6A), and exhibits low-sequence identity between mGluR2 and mGluR3. The mGluR3 ST-rich region contains 6 overlapping Px(x)PxxP/E/D full phospho-codes, as defined based on an arrestin-bound rhodopsin crystal structure (Zhou et al., 2017), whereas the mGluR2 CTD contains 0 phospho-codes (Figure 6A). Consistent with our results (Figures 1 and 2), mGluR7 and mGluR8 have full phospho-codes within the membrane proximal region of their CTDs, whereas mGluR4 has only 1 phosphorylation code in its distal CTD (Figure S7A). However, both mGluR1 and mGluR5 contain many phospho-codes along their extended CTDs, indicating that the mere presence of phospho-codes is not sufficient to ensure β-arr coupling (Figure S7A).

We first deleted the ST-rich region from mGluR3 (mGluR3-ΔST) and observed a large decrease in receptor internalization (Figures 6B–6D) and β-arr recruitment (Figures S7C–S7E), despite normal surface expression (Figure S7B). Introducing the ST-rich region of mGluR2 into mGluR3 (mGluR3-mGluR2ST) also attenuated internalization (Figures 6B–6D) and β-arr recruitment (Figures S7C–S7E). Interestingly, mGluR3-ΔST exhibited higher levels of internalization than mGluR3-mGluR2ST (Figure 6C), providing further evidence that the mGluR2 CTD has inhibitory properties. In contrast, mGluR2-mGluR3ST showed robust internalization (Figures 6B–6D) and β-arr recruitment (Figures S7C–S7E). Altogether, these results indicate that the ST-rich region of mGluR3 contains residues that are important for its desensitization.

Consistent with the requirement of a functional GRK2 kinase domain (Figure 4F), the ST-rich region plays a role in the rapid desensitization of mGluR3. GRK2 expression did not enhance the rapid desensitization of GIRK currents mediated by mGluR3-ΔST or mGluR3-mGluR2ST but did enhance desensitization of currents mediated by mGluR2-mGluR3ST (Figures 6E and 6F; Figures S7F and S7G). Moreover, GRK2 expression decreased the amplitudes of mGluR2-mGluR3ST-mediated currents (Figure S7H).

To identify key residues, we mutated Ser and Thr residues in the ST-rich region to Ala and found that mutating all ten (10xA) abolished mGluR3 internalization and β-arr recruitment (Figure 6G; Figures S7I–S7K). mGluR3-10xA also showed a lack of sensitivity to GRK2 in GIRK measurements (Figures S7L and S7M). Mutating either the first six ($6xA_{v1}$) or last six ($6xA_{v2}$)

(C–E) Representative TIRF images showing a lack of β-arr2 puncta for mGluR2 (C) but a high density of β-arr2 puncta generated by activation of mGluR3 (D) and β_2AR (E). Line scans reveal colocalization of receptor (red) and β-arr2 (green) puncta. Black arrows denote overlapping peaks.
(F) Summary bar graph of receptor and β-arr2 puncta densities under basal conditions and agonist treatment. Paired t tests, *p = 0.03 for mGluR3 basal and *p = 0.01 for mGluR3 + Glu.
(G) Quantification of the percentage of β-arr2 puncta that are colocalized with either mGluR3 (under basal or +Glu conditions) or β_2AR (+Iso) puncta. Unpaired t tests, *p = 0.03 for mGluR3 basal versus +Glu and ***p = 0.0005 for mGluR3 + Glu versus β_2AR + Iso.
(H) Left, representative TIRF images showing that mGluR3 activation leads to β-arr2 puncta that colocalize extensively with the CCP marker, CLC. Right, intensity line scan through the white dotted line on the images that shows overlapping β-arr2 (green) and CLC (red) peaks, denoted by the black arrows.
(I) Schematic of the working model for β-arr coupling with mGluR3.
Error bars show SEM. Scale bar, 10 μm (B–E) or 5 μm (H). Number of fields of cells (A) or cells (F and G) analyzed is in parentheses.

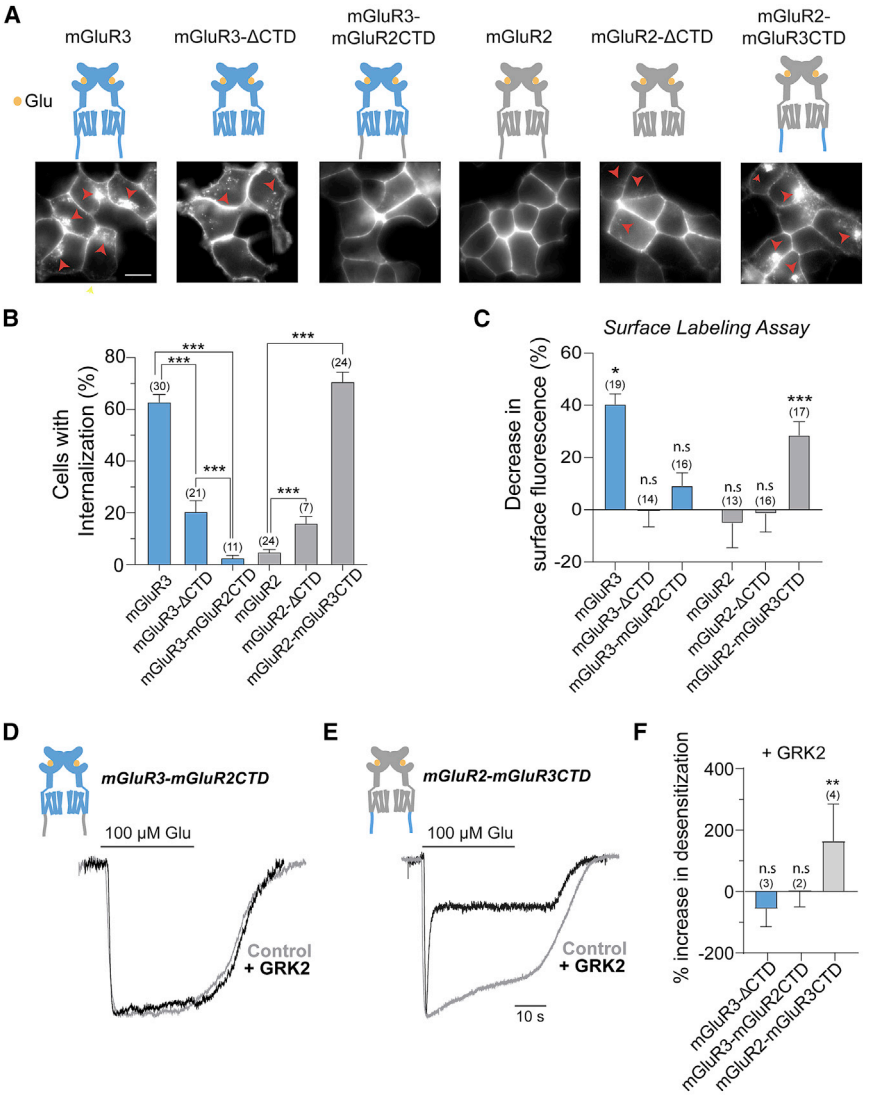

Figure 5. The C-terminal domains mediate differential internalization and rapid desensitization of mGluRs

(A) Top, illustrations of CTD deletions and chimeras for mGluR2 and mGluR3. Bottom, representative images of HEK293T cells expressing SNAP-tagged receptors and incubated for 30 min in Glu. Red arrowheads show internalized receptors. Scale bar, 10 μm.

(B) Quantification of the percentage of cells that exhibit internalization of the various CTD variants. *** indicates statistical significance. Unpaired t test, $p < 0.0001$ for mGluR3 versus mGluR3-ΔCTD, $p < 0.0001$ for mGluR3 versus mGluR3-mGluR2CTD, $p < 0.0001$ for mGluR2 versus mGluR2-ΔCTD, $p < 0.0001$ for mGluR2 versus mGluR2-mGluR3CTD, and $p = 0.0005$ for mGluR3-ΔCTD versus mGluR2.

(C) Quantification of surface fluorescence reduction following Glu application, where the control was no Glu. Unpaired t tests, *$p = 0.03$ mGluR3 and ***$p < 0.0001$ for mGluR2-mGluR3CTD.

(D and E) Representative GIRK current traces for mGluR3-mGluR2CTD (D) and mGluR2-mGluR3CTD (E) with and without GRK2 overexpression.

(F) Summary plot showing the percentage increase in desensitization of GIRK currents in the presence of GRK2 overexpression. Unpaired t test versus no GRK2 overexpression condition, **$p = 0.005$.

Error bars show SEM. Number of fields of cells analyzed (B and C) or independent experiments (F) is in parentheses.

Ser/Thr residues also abolished internalization and β-arr recruitment (Figure 6G; Figures S7I–S7K), while mutating the first four (4xA) Ser/Thr residues produced partial effects (Figure 6G; Figures S7I–S7K). This shows that efficient β-arr coupling and subsequent internalization of mGluR3 requires multiple Ser and Thr residues.

Based on our findings, we propose a model for mGluR3 desensitization (Figure 6H) in which GRK2 is specifically recruited to active mGluR3 by binding to the transmembrane core and recognizing the ST-rich region of the CTD via its kinase domain. This recruitment allows GRK2 to phosphorylate CTD residues and to bind $G_{\beta\gamma}$ to desensitize GIRK channels and other effectors. Phosphorylated mGluR3 can then recruit β-arr to initiate internalization of the receptor. Critically, receptor subtype specificity between group II mGluRs is mediated primarily by a differential ability to recruit GRK2 directly to the receptor, and this ability is primarily governed by the identity of the CTD.

A cancer-associated CTD mutation enhances β-arrestin coupling and internalization of mGluR3

A large-scale mutational analysis of GPCRs identified mutations in mGluR3 in 17% of melanoma tumor samples (Prickett et al., 2011). One mutation, G848E, is located within the ST-rich region (Figure 7A), raising the possibility that this may modify β-arr coupling. Consistent with this hypothesis, we found that cells express mGluR3-G848E to similar levels as WT (Figure S8A) but exhibit enhanced internalization, even in the absence of glutamate stimulation (Figures 7A and 7B; Figure S8B). The basal internalization of mGluR3-G848E was blocked only following 3 h of incubation in ML289, indicating that it likely depends on some accumulation of phosphorylation (Figure S8C). The glutamate-dependent internalization of G848E was only partially sensitive to cmpd101 treatment (Figures S8D and S8E), and full block required prolonged incubation with cmpd101 and ML289 (Figure S8E). These data suggest that the threshold for sufficient CTD phosphorylation to initiate internalization is lowered in this mutant.

Consistent with internalization data, mGluR3-G848E was able to recruit β-arr2 to the surface in the absence of glutamate application and to higher levels with glutamate (Figure 7A;

CellPress
OPEN ACCESS

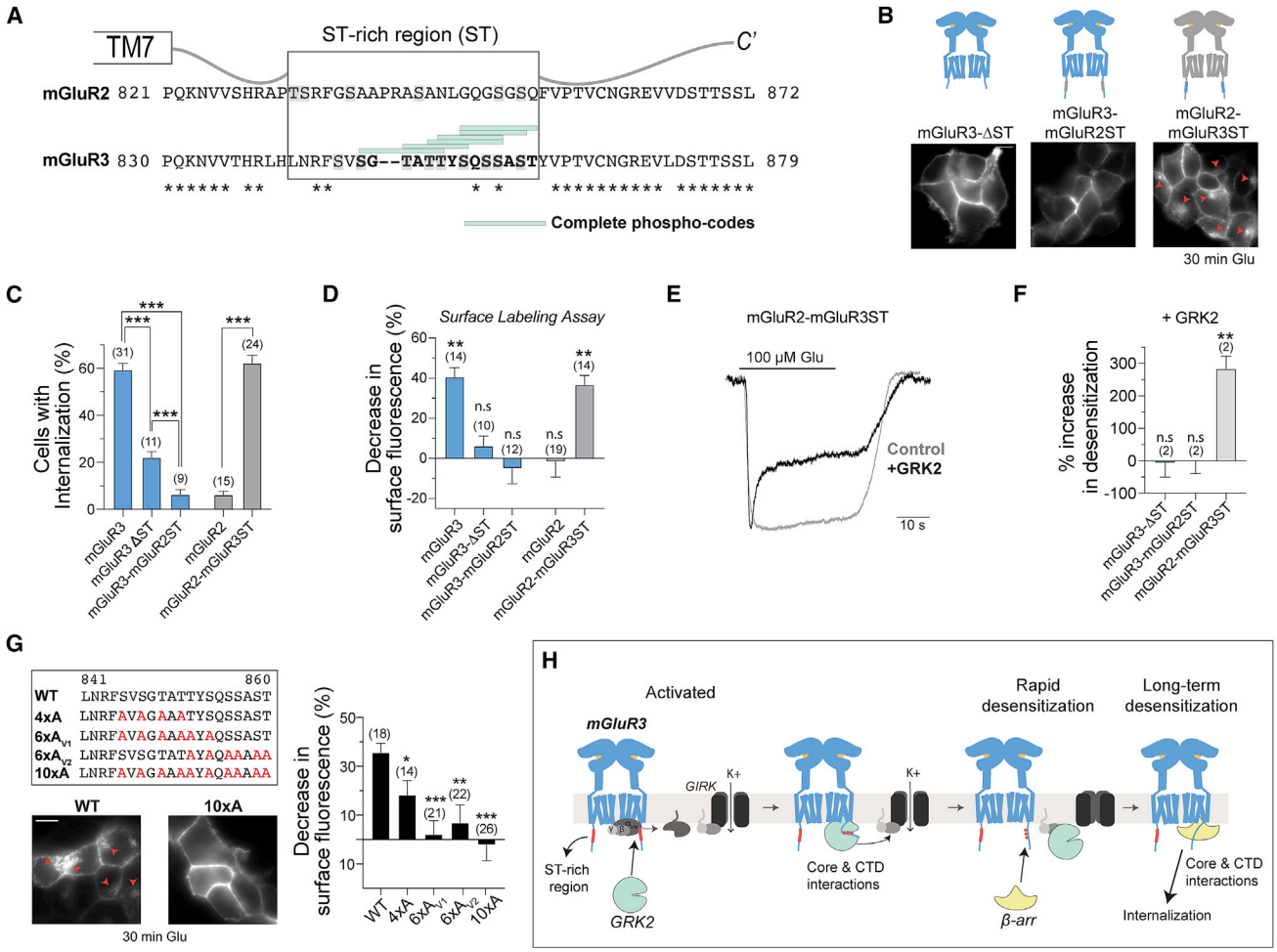

Figure 6. A Ser/Thr-rich stretch of the mGluR3CTD controls GRK- and β-arrestin-dependent internalization and rapid desensitization

(A) Sequence alignment of the CTDs of mGluR2 and mGluR3 displaying the Ser/Thr (ST)-rich sequence and phospho-codes.

(B) Top, illustrations of ST-rich region deletion and chimeric constructs. Bottom, representative images of HEK293T cells expressing SNAP-tagged receptor constructs and incubated in 1 mM Glu for 30 min.

(C) Quantification of the percentage of cells that exhibit internalization of the various ST sequence variants. Unpaired t tests, ***$p < 0.0001$ for all comparisons made.

(D) Quantification of the percentage of the internalized surface receptor population as determined by the surface labeling assay, in which the control was no Glu. Unpaired t tests, **$p = 0.003$ for mGluR3 and **$p = 0.001$ for mGluR2-mGluR3ST.

(E) Recordings showing the GRK2 sensitivity of mGluR2-mGluR3ST-mediated GIRK currents.

(F) Summary plot showing the percentage increase in desensitization of GIRK currents with GRK2 overexpression. Unpaired t test versus no GRK2 overexpression, **$p = 0.006$.

(G) Top left, sequence alignments of the ST-rich region of mGluR3, showing the residues that were mutated to Ala. Bottom left, images of cells expressing either WT mGluR3 or mGluR3-10xA following 30 min of 1 mM Glu treatment. Red arrows point to internalized receptors. Right, summary bar graph showing the percentage decrease in surface fluorescence following treatment with 1 mM Glu across mutants. Unpaired t tests, *$p = 0.02$ for WT versus 4xA, ***$p < 0.0001$ for WT versus 6xA$_{V1}$, **$p = 0.003$ for WT versus 6xA$_{V2}$, and ***$p < 0.0001$ for WT versus 10xA.

(H) Working model of GRK2- and β-arr-mediated rapid and long-term desensitization of mGluR3.

Error bars show SEM. Scale bars, 10 μm. Number of fields of cells analyzed (B, D, and G) or independent experiments (F) is shown in parentheses.

Figures S8F–S8H). Despite the apparent enhanced interaction, β-arr remained on the surface following internalization of mGluR3-G848E (Figure S8I), indicating that this mutation does not alter the trafficking of mGluR3/β-arr complexes. In contrast to the effects on β-arr coupling, mGluR3-G848E showed slightly decreased basal desensitization and similar sensitivity to GRK2 (Figures S8J–S8L). mGluR3-G848E produced larger GIRK currents than WT (Figure S8L), suggesting that effects on G protein coupling may also exist.

Tuning β-arrestin coupling of mGluR3 via mutations to the TMD and CTD

We investigated the interactions of β-arr and mGluR3 by asking how modifications to the receptor alter coupling. We first asked

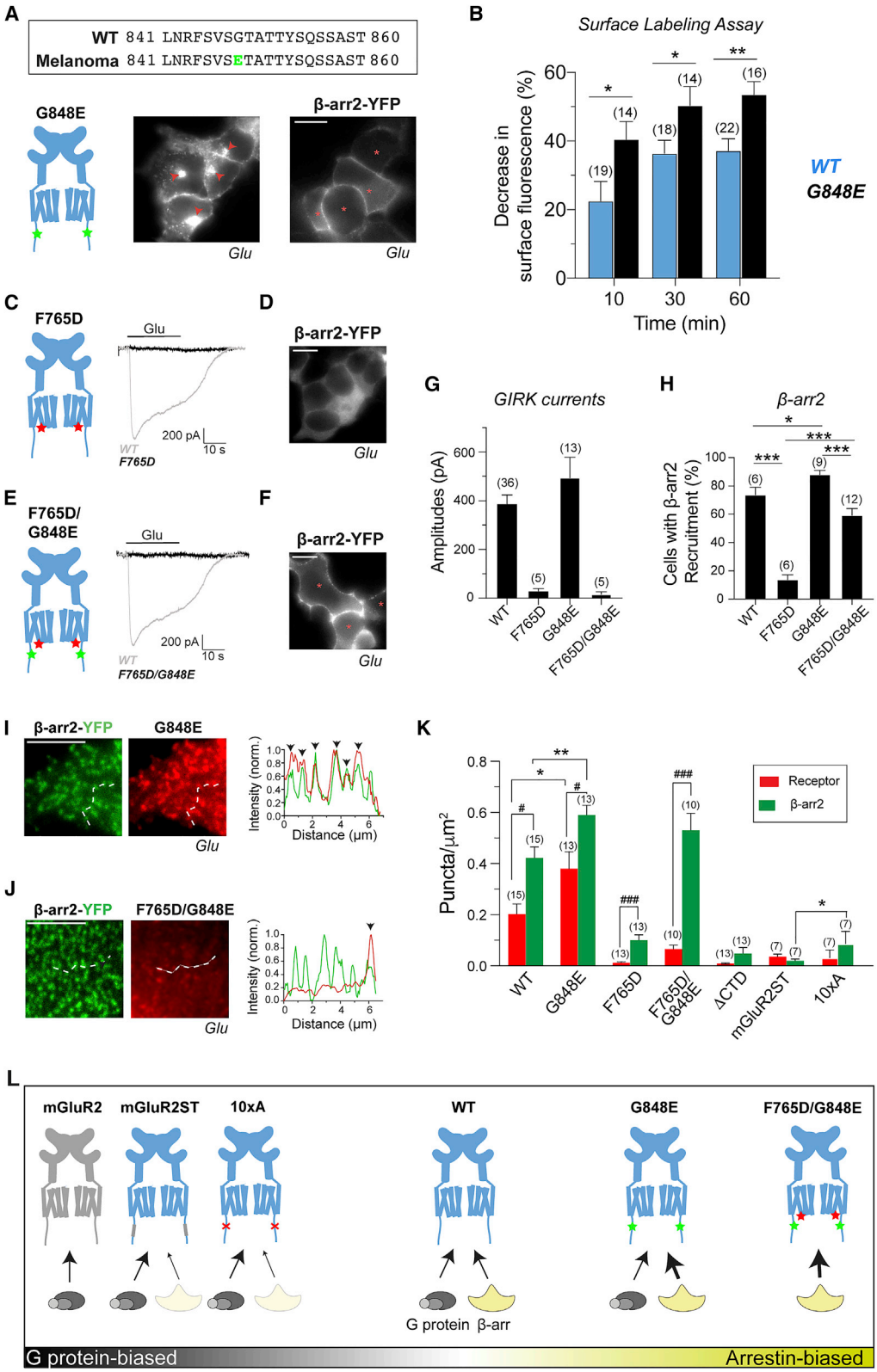

(legend on next page)

whether β-arr interacts with the G protein binding site of the TMD core of mGluR3, because such an interaction has been shown for GPCRs (Huang et al., 2020; Staus et al., 2020; Hilger et al., 2018). We first mutated a conserved phenylalanine (F765D) in intracellular loop 3 that is known to abolish G protein coupling across mGluRs (Figure S8M) (Francesconi and Duvoisin, 1998; Kniazeff et al., 2004; Levitz et al., 2016) and observed undetectable GIRK currents (Figure 7C), despite normal expression (Figure S8N). F765D also nearly abolished the ability of mGluR3 to recruit β-arr to the surface following activation (Figure 7D) and exhibited negligible internalization (Figures S8O and S8P), indicating that β-arr interacts with the TMD core of mGluR3 in a similar way to G proteins. Given the enhanced coupling to β-arr by mGluR3-G848E, we asked whether introduction of the F765D mutation into this mutant background would prevent β-arr coupling. The double mutant (G848E/F765D) did not produce GIRK currents (Figure 7E) but, surprisingly, showed substantial surface recruitment of β-arr to nearly WT levels (Figure 7F). This indicates that the enhanced CTD coupling of G848E can overcome the weak TMD coupling of F765D to produce a β-arr-biased mutant (Figures 7G and 7H).

To further understand the effects of TMD and CTD perturbations, we turned to TIRF imaging, with which we observed various levels of glutamate-induced receptor and β-arr2 puncta for WT mGluR3, G848E, F765D, F765D/G848E, mGluR3-mGluR2ST, mGluR3-10xA, and mGluR3-ΔCTD (Figures 7I–7K; Figure S8Q). Consistent with receptor internalization and β-arr recruitment data (Figure 7), G848E produced higher levels of receptor and β-arr2 puncta compared with WT (Figures 7I and 7K). However, β-arr2 showed a slightly higher degree of colocalization with G848E (Figure S8R), suggesting a more stable form of coupling. In addition, under basal conditions, G848E showed substantially more β-arr2 puncta than receptor puncta (Figure S8S), consistent with what was seen with WT (Figure 3F). As expected, F765D/G848E also produced a high density of β-arr2 puncta but, interestingly, a lower level of receptor puncta (Figures 7J and 7K). Correspondingly, a low level of β-arr puncta colocalized with the double mutant (Figure S8R). This lack of apparent tight association with β-arr may explain why F765D/G848E internalization is weaker than WT (Figure S7K).

The density of receptor and β-arr2 puncta was low but higher than that seen with mGluR2 for both mGluR3-F765D and mGluR3-ΔCTD (mGluR2 = 0.006 ± 0.002 puncta/μm^2, mGluR3-F765D = 0.10 ± 0.02 puncta/μm^2, and mGluR3-ΔCTD = 0.04 ± 0.01 puncta/μm^2) (Figure 7K; Figure S8Q). For all constructs that weakly recruit β-arr, a higher density was observed for β-arr2 compared with the receptor (Figure 7K) and the degree of colocalization between β-arr2 and mGluR3 was very low (Figure S8R), suggesting that weak β-arr coupling typically proceeds through a catalytic mechanism (Eichel et al., 2016, 2018).

Having developed a β-arr-biased mGluR3, we sought to define a G protein-biased variant. We observed minimal receptor and β-arr puncta formation and colocalization with glutamate for both mGluR3-mGluR2ST and mGluR3-10xA (Figure 7K; Figures S8P and S8R), making mGluR3-mGluR2ST and mGluR3-10xA good candidates. As summarized in Figure 7L, this analysis led us to identify a range of mGluR3 variants that show different degrees of bias toward G protein and β-arr coupling, as well as variability in the mode of β-arr coupling (i.e., scaffold versus catalytic).

DISCUSSION

Functional diversity of mGluRs

We report a comparative analysis of the diverse desensitization and trafficking properties of mGluRs, in which only a subset of subtypes undergoes β-arr-mediated internalization, with mGluR3 showing the most pronounced effects. In a recent high-throughput screen of GPCR/transducer coupling, all mGluR subtypes tested (mGluR2, mGluR4, mGluR5, mGluR6, and mGluR8) showed little to no β-arr recruitment, although mGluR3 was not included (Avet et al., 2020). However, another study (Lee et al., 2019) used biochemical assays to show coupling between mGluR7 and β-arr. Our data were consistent with β-arr-driven internalization of a subset of group III mGluRs, with the major exception of mGluR4, which undergoes β-arr-independent constitutive internalization. We found no evidence for β-arr-dependent internalization of group I mGluRs, in contrast to some previous reports (Dale et al., 2001; Mundell et al., 2001) but in line with the aforementioned screen (Avet et al., 2020). Two studies used knockout mice to report that mGluR5-mediated

Figure 7. Cancer-associated G848E mutation in the mGluR3CTD enables the identification of biased mGluR3 variants

(A) Top, mutation G848E (green) within the ST-rich region of the mGluR3CTD is associated with melanoma. Bottom, mGluR3-G848E exhibits internalization and surface recruitment of β-arr2.

(B) Surface labeling assay summary graph showing enhanced internalization for G848E compared with WT. Unpaired t tests, *p = 0.03 for 10 min, *p = 0.04 for 30 min, and **p = 0.003 for 60 min.

(C and D) mGluR3-F765D is unable to produce Glu-induced GIRK channel activation (C) or β-arr2-YFP recruitment (D).

(E and F) mGluR3-F765D/G848E is unable to produce Glu-induced GIRK channel activation (E) but exhibits β-arr2 recruitment (F).

(G and H) Summary bar graphs showing the efficiency of G protein activation as detected via GIRK currents (G) and the efficiency of β-arr recruitment as measured by percentage cell analysis (H). Unpaired t tests, ***p < 0.0001 for WT versus F765D, *p = 0.02 for WT versus G848E, ***p = 0.0001 for G848E versus F765D/G848E, and ***p < 0.0001 for F765D versus F765D/G848E.

(I and J) Differential receptor and β-arr2 puncta formation for G848E (I) and F765D/G848E (J) mutants.

(K) Summary of mGluR3 and β-arr2 puncta density produced across receptor variants. # indicates statistical significance. Paired t tests, ###p = 0.0008 for WT, ##p = 0.008 for G848E, and ###p = 0.0008 for F765D. * indicates statistical significance. Unpaired t tests, *p = 0.04 for WT versus G848E receptor bars, **p = 0.002 for WT versus G848E β-arr2 bars, and **p = 0.008 for mGluR2ST versus 10xA β-arr2 bars. n = 15 cells for WT, 13 for G848E, 13 for F765D, 10 for F765D/G848E, 13 for ΔCTD, 7 for mGluR2ST, 7 for 10xA).

(L) Schematic showing the relative G protein- and β-arr-coupling propensities of group II mGluR variants.

Scale bar, 10 μm (A, C, and E) or 5 μm (I and J). Number of fields of cells analyzed (B and H), cells recorded from (G), or cells analyzed (K) is in parentheses.

hippocampal long-term depression partially depends on β-arr (Eng et al., 2016; Stoppel et al., 2017), suggesting that a direct or indirect functional interaction between group I mGluRs and β-arr can occur. GPCRs can be internalized via other mechanisms, which may involve various kinases and protein scaffolding complexes, as shown for mGluR5 and the scaffold Shank (Scheefhals et al., 2019). Thus, future work is needed to analyze mGluR internalization and β-arr-mediated signaling in biological contexts (Suh et al., 2018; Reiner and Levitz, 2018).

We also show that many mGluRs are sensitive to GRK2-mediated rapid functional desensitization. This includes mGluR1 and mGluR5, which are resistant to GRK- and β-arr-mediated internalization under the conditions tested here. Previous studies showed mixed results for functional GRK sensitivity of group I mGluRs, with some reporting kinase-dependent effects (Dhami et al., 2002, 2004; Sorensen and Conn, 2003) versus kinase-independent effects (Dale et al., 2000; Dhami et al., 2002; Ribeiro et al., 2009) using endpoint assays. Using time-resolved measurements of calcium responses, we show that group I mGluR signaling is rapidly desensitized on the ~10 s timescale by GRK2 in a kinase-independent manner. In contrast to group I mGluRs, although mGluR7 shows GRK- and β-arr-dependent internalization, it eluded rapid GRK2-mediated functional effects in our patch-clamp assay. These data suggest that distinct modes of GRK coupling are required for rapid versus slower desensitization effects. An important caveat of our analysis is that although we have focused on GRK2, other GRK subtypes that have distinct domain architectures (Komolov and Benovic, 2018) may show unique effects.

Overall, with the exception of mGluR2, which we found is uniquely resistant to all forms of desensitization tested, all mGluRs show varying degrees and forms of regulation (Figure 3L). This suggests that distinct regulatory properties are a major aspect of the functional diversity of mGluRs. Recent work has revealed that mGluRs heterodimerize (Doumazane et al., 2011; Lee et al., 2020), likely providing further desensitization diversity.

Differential GRK- and arrestin-coupling mechanisms

Our mechanistic analysis focused on group II mGluRs, which have typically been treated monolithically because of their high degree of sequence identity and difficulty distinguishing them with pharmacological compounds or antibodies. We find that mGluR3, but not mGluR2, is subject to rapid functional desensitization and internalization. These differences are underscored by different abilities to couple to GRKs and β-arr and are primarily encoded within the mGluR CTDs.

Classically, GRKs are thought to be recruited to the membrane via free $G_{\beta\gamma}$ proteins released following receptor activation, which then enables coupling to the GPCR (Pitcher et al., 1992). Our data, in which only mGluR3 and mGluR8 are desensitized despite mGluR2, mGluR4, and mGluR7 also producing free $G_{\beta\gamma}$, argue for a mechanism, in which cytosolic GRK is recruited directly to the active receptor instead of to $G_{\beta\gamma}$. This is consistent with GRK2-dependent mGluR3 internalization in the presence of PTX, which prevents the release of $G_{\beta\gamma}$. Recruitment of GRK2 directly to the activated receptor could explain the GPCR subtype specificity of GRK2-mediated GIRK desensitization reported here and previously (Raveh et al., 2010), as well as the PTX-insensitive surface recruitment of GRK2 reported in the same study. A recent study (Stoeber et al., 2020) found that GRK2 recruitment by the kappa-opioid receptor was abolished by PTX for etorphine, but not dynorphin A, showing that the mechanism of GRK recruitment can be both agonist and receptor specific. Our data also argue that critical interactions take place between the mGluR3 CTD and the kinase domain of GRK2 to mediate rapid desensitization. Swapping the ST-rich region of the CTDs swapped the ability of mGluR2 and mGluR3 to undergo GRK2-mediated desensitization, and kinase-dead GRK2 was unable to desensitize mGluR3 signaling. This is in contrast to what was reported previously (Raveh et al., 2010) for A1R, in which the kinase-dead mutant produced desensitization, suggesting that different GPCRs differ in their dependence on interactions with the GRK kinase domain. mGluR8 also showed GRK2-mediated functional desensitization that was abolished in the kinase-dead mutant, suggesting a mode of interaction similar to that of mGluR3. Our data argue for a bitopic interaction between GRKs and both the transmembrane domain and the ST-rich region of the CTD of mGluR3 (or mGluR8) in a manner that depends on an intact GRK kinase domain. This is consistent with a biochemical study that revealed extensive interactions between GRK5 and both intracellular loops and the CTD of the β_2AR (Komolov et al., 2017). Studies have also shown that GRK2 recruitment and rapid desensitization of the mu-opioid receptor require intact CTD phospho-sites (Arttamangkul et al., 2019; Leff et al., 2020; Miess et al., 2018).

Our data show that mGluR3 falls roughly into the class A distinction of GPCRs based on its transient β-arr coupling. However, unlike many class A GPCRs, such as β_2AR, mGluR3 showed no preference between β-arr subtypes. Furthermore, our TIRF imaging supports recent studies (Eichel et al., 2016, 2018) showing that catalytic coupling can occur, in which a single GPCR briefly interacts with a β-arr that subsequently remains bound to the membrane and clusters at CCPs. We find that the degree of activation of mGluR3, whether it is via the low ambient levels of glutamate that produce basal activity or saturating 1 mM glutamate, determines the degree of scaffold versus catalytic coupling. Basal activity led to more catalytic coupling, whereas saturating glutamate produced more scaffold coupling with a higher proportion of colocalized mGluR3 and β-arr. Both the extent of occupancy of the active TMD conformation of the receptor and the degree of CTD phosphorylation likely determine the lifetime of the receptor-transducer complex. Thus, the level and dynamics of extracellular glutamate likely shape the mode of β-arr coupling for mGluR3 in physiological settings.

Our finding that mGluR3, but not mGluR2, undergoes agonist-dependent internalization into endosomes is consistent with a mobility study that found mGluR3 accumulation at CCPs (Yanagawa et al., 2018) but did not investigate receptor internalization. Following internalization, we find that mGluR3 primarily recycles back to the surface with minimal occupancy of lysosomes, suggesting that degradation is not a major downstream consequence of internalization. Future work will be needed to identify the proteins that mediate mGluR3 trafficking to different cellular compartments, the roles of different phosphorylation sites in controlling the trafficking itinerary, and whether endosomal mGluR3 can signal.

Physiological relevance of differential regulation of group II mGluRs

Our results suggest that major differences in downstream signaling properties likely exist between group II mGluRs. The ability of mGluR3 to couple to β-arr opens the possibility of signaling to various effectors, including ERK, AKT, and JNKs (Peterson and Luttrell, 2017). Importantly, many of these same effectors are also targeted via G protein-dependent pathways, and debate exists over the relative contributions of G protein and β-arr pathways to ERK activation (Luttrell et al., 2018; O'Hayre et al., 2017).

Our results also have implications for the roles of group II mGluRs in their classical location of excitatory synapses, where we anticipate distinct surface lifetimes and signaling dynamics for mGluR2 and mGluR3. One possibility is that the relative desensitization of group II mGluRs can determine their effects following activation over synaptic plasticity-relevant timescales of minutes to hours. For example, studies of the effects of acute stress on group II mGluRs in the cortex have found downregulation of mGluR3, but not mGluR2 (Joffe et al., 2019). Further work is needed to address a potential role for GRK and β-arr coupling and dynamic trafficking of mGluR3 in intact physiological settings.

Finally, our findings highlight the need for techniques to dissect β-arr versus G protein signaling of mGluR3, especially in physiologically relevant settings. The ability of mGluR3 to couple to β-arr and G proteins opens the possibility that biased ligands may be developed. Recent work (Ellaithy et al., 2020; Gutzeit et al., 2019) has revealed heterogeneity in the kinetics, efficacy, and chemical scaffolds of allosteric modulators, suggesting that sufficient chemical and conformational complexity exists to harness pharmacology for these purposes. Alternatively, the G protein- and β-arr-biased mGluR3 variants reported here (Figure 7) may be useful for probing the relative roles of each transducer in mGluR3 biology. In the long term, the ability to combine biased mutants with genetically targeted photopharmacology, as we reported for mGluR3 (Acosta-Ruiz et al., 2020), offers a potentially powerful approach for dissecting G protein versus β-arr signaling *in vivo*.

STAR★METHODS

Detailed methods are provided in the online version of this paper and include the following:

- KEY RESOURCES TABLE
- RESOURCE AVAILABILITY
  - Lead contact
  - Materials availability
  - Data and code availability
- EXPERIMENTAL MODEL AND SUBJECT DETAILS
- METHOD DETAILS
  - Molecular biology
  - Cell culture and transfection
  - Surface labeling assay
  - Internalization and arrestin recruitment assays
  - Recycling assay
  - Confocal microscopy
  - Total internal reflection fluorescence microscopy
  - Patch clamp electrophysiology
  - Calcium imaging
- QUANTIFICATION AND STATISTICAL ANALYSIS

SUPPLEMENTAL INFORMATION

Supplemental information can be found online at https://doi.org/10.1016/j.celrep.2021.109050.

ACKNOWLEDGMENTS

We thank Drs. Frederick R. Maxfield, Timothy E. McGraw, Jeremy S. Dittman, David Eliezer, Robert J. Lefkowitz, and Seungkirl Ahn for discussion and critical reagents. N.A. is supported by a National Science Foundation (NSF) Graduate Research Fellowship. J.L. is supported by an R35 grant (R35 GM124731) from NIGMS and the Rohr Family Research Scholar Award.

AUTHOR CONTRIBUTIONS

N.A. designed and conducted experiments, analyzed data, and wrote the manuscript. A.A.-R. and G.X. designed, conducted, and analyzed calcium imaging experiments. J.L. designed experiments, analyzed data, and wrote the manuscript.

DECLARATION OF INTERESTS

The authors declare no competing interests.

Received: January 12, 2021
Revised: March 4, 2021
Accepted: April 7, 2021
Published: April 27, 2021

REFERENCES

Abdullah, N., Beg, M., Soares, D., Dittman, J.S., and McGraw, T.E. (2016). Downregulation of a GPCR by β-Arrestin2-Mediated Switch from an Endosomal to a TGN Recycling Pathway. Cell Rep. *17*, 2966–2978.

Acosta-Ruiz, A., Gutzeit, V.A., Skelly, M.J., Meadows, S., Lee, J., Parekh, P., Orr, A.G., Liston, C., Pleil, K.E., Broichhagen, J., and Levitz, J. (2020). Branched Photoswitchable Tethered Ligands Enable Ultra-efficient Optical Control and Detection of G Protein-Coupled Receptors *In Vivo*. Neuron *105*, 446–463.e13.

Ahn, S., Shenoy, S.K., Wei, H., and Lefkowitz, R.J. (2004). Differential kinetic and spatial patterns of beta-arrestin and G protein-mediated ERK activation by the angiotensin II receptor. J. Biol. Chem. *279*, 35518–35525.

Arttamangkul, S., Leff, E.R., Koita, O., Birdsong, W.T., and Williams, J.T. (2019). Separation of Acute Desensitization and Long-Term Tolerance of μ-Opioid Receptors Is Determined by the Degree of C-Terminal Phosphorylation. Mol. Pharmacol. *96*, 505–514.

Avet, C., Mancini, A., Breton, B., Le Gouill, C., Hauser, A.S., Normand, C., Kobayashi, H., Gross, F., Hogue, M., Lukasheva, V., et al. (2020). Selectivity Landscape of 100 Therapeutically Relevant GPCR Profiled by an Effector Translocation-Based BRET Platform. bioRxiv. https://doi.org/10.1101/2020.04.20.052027.

Cahill, T.J., 3rd, Thomsen, A.R., Tarrasch, J.T., Plouffe, B., Nguyen, A.H., Yang, F., Huang, L.Y., Kahsai, A.W., Bassoni, D.L., Gavino, B.J., et al. (2017). Distinct conformations of GPCR-β-arrestin complexes mediate desensitization, signaling, and endocytosis. Proc. Natl. Acad. Sci. USA *114*, 2562–2567.

Carman, C.V., Barak, L.S., Chen, C., Liu-Chen, L.Y., Onorato, J.J., Kennedy, S.P., Caron, M.G., and Benovic, J.L. (2000). Mutational analysis of Gbetagamma and phospholipid interaction with G protein-coupled receptor kinase 2. J. Biol. Chem. *275*, 10443–10452.

Dale, L.B., Bhattacharya, M., Anborgh, P.H., Murdoch, B., Bhatia, M., Nakanishi, S., and Ferguson, S.S. (2000). G protein-coupled receptor kinase-mediated desensitization of metabotropic glutamate receptor 1A protects against cell death. J. Biol. Chem. *275*, 38213–38220.

Dale, L.B., Bhattacharya, M., Seachrist, J.L., Anborgh, P.H., and Ferguson, S.S. (2001). Agonist-stimulated and tonic internalization of metabotropic glutamate receptor 1a in human embryonic kidney 293 cells: agonist-stimulated endocytosis is beta-arrestin1 isoform-specific. Mol. Pharmacol. *60*, 1243–1253.

DeWire, S.M., Ahn, S., Lefkowitz, R.J., and Shenoy, S.K. (2007). Beta-arrestins and cell signaling. Annu. Rev. Physiol. *69*, 483–510.

Dhami, G.K., Anborgh, P.H., Dale, L.B., Sterne-Marr, R., and Ferguson, S.S. (2002). Phosphorylation-independent regulation of metabotropic glutamate receptor signaling by G protein-coupled receptor kinase 2. J. Biol. Chem. *277*, 25266–25272.

Dhami, G.K., Dale, L.B., Anborgh, P.H., O'Connor-Halligan, K.E., Sterne-Marr, R., and Ferguson, S.S. (2004). G Protein-coupled receptor kinase 2 regulator of G protein signaling homology domain binds to both metabotropic glutamate receptor 1a and Galphaq to attenuate signaling. J. Biol. Chem. *279*, 16614–16620.

Doumazane, E., Scholler, P., Zwier, J.M., Trinquet, E., Rondard, P., and Pin, J.P. (2011). A new approach to analyze cell surface protein complexes reveals specific heterodimeric metabotropic glutamate receptors. FASEB J. *25*, 66–77.

Dutar, P., Vu, H.M., and Perkel, D.J. (1999). Pharmacological characterization of an unusual mGluR-evoked neuronal hyperpolarization mediated by activation of GIRK channels. Neuropharmacology *38*, 467–475.

Eichel, K., Jullié, D., and von Zastrow, M. (2016). β-Arrestin drives MAP kinase signalling from clathrin-coated structures after GPCR dissociation. Nat. Cell Biol. *18*, 303–310.

Eichel, K., Jullié, D., Barsi-Rhyne, B., Latorraca, N.R., Masureel, M., Sibarita, J.B., Dror, R.O., and von Zastrow, M. (2018). Catalytic activation of β-arrestin by GPCRs. Nature *557*, 381–386.

Ellaithy, A., Gonzalez-Maeso, J., Logothetis, D.A., and Levitz, J. (2020). Structural and Biophysical Mechanisms of Class C G Protein-Coupled Receptor Function. Trends Biochem. Sci. *45*, 1049–1064.

Emery, A.C., Pshenichkin, S., Takoudjou, G.R., Grajkowska, E., Wolfe, B.B., and Wroblewski, J.T. (2010). The protective signaling of metabotropic glutamate receptor 1 Is mediated by sustained, beta-arrestin-1-dependent ERK phosphorylation. J. Biol. Chem. *285*, 26041–26048.

Eng, A.G., Kelver, D.A., Hedrick, T.P., and Swanson, G.T. (2016). Transduction of group I mGluR-mediated synaptic plasticity by β-arrestin2 signalling. Nat. Commun. *7*, 13571.

Erdtmann-Vourliotis, M., Mayer, P., Ammon, S., Riechert, U., and Höllt, V. (2001). Distribution of G-protein-coupled receptor kinase (GRK) isoforms 2, 3, 5 and 6 mRNA in the rat brain. Brain Res. Mol. Brain Res. *95*, 129–137.

Ferguson, S.S., Downey, W.E., 3rd, Colapietro, A.M., Barak, L.S., Ménard, L., and Caron, M.G. (1996). Role of beta-arrestin in mediating agonist-promoted G protein-coupled receptor internalization. Science *271*, 363–366.

Fourgeaud, L., Bessis, A.S., Rossignol, F., Pin, J.P., Olivo-Marin, J.C., and Hémar, A. (2003). The metabotropic glutamate receptor mGluR5 is endocytosed by a clathrin-independent pathway. J. Biol. Chem. *278*, 12222–12230.

Francesconi, A., and Duvoisin, R.M. (1998). Role of the second and third intracellular loops of metabotropic glutamate receptors in mediating dual signal transduction activation. J. Biol. Chem. *273*, 5615–5624.

Francesconi, A., Kumari, R., and Zukin, R.S. (2009). Regulation of group I metabotropic glutamate receptor trafficking and signaling by the caveolar/lipid raft pathway. J. Neurosci. *29*, 3590–3602.

Gainetdinov, R.R., Premont, R.T., Bohn, L.M., Lefkowitz, R.J., and Caron, M.G. (2004). Desensitization of G protein-coupled receptors and neuronal functions. Annu. Rev. Neurosci. *27*, 107–144.

Gillooly, D.J., Morrow, I.C., Lindsay, M., Gould, R., Bryant, N.J., Gaullier, J.M., Parton, R.G., and Stenmark, H. (2000). Localization of phosphatidylinositol 3-phosphate in yeast and mammalian cells. EMBO J. *19*, 4577–4588.

Gutzeit, V.A., Thibado, J., Stor, D.S., Zhou, Z., Blanchard, S.C., Andersen, O.S., and Levitz, J. (2019). Conformational dynamics between transmembrane domains and allosteric modulation of a metabotropic glutamate receptor. eLife *8*, e45116.

Hilger, D., Masureel, M., and Kobilka, B.K. (2018). Structure and dynamics of GPCR signaling complexes. Nat. Struct. Mol. Biol. *25*, 4–12.

Huang, W., Masureel, M., Qu, Q., Janetzko, J., Inoue, A., Kato, H.E., Robertson, M.J., Nguyen, K.C., Glenn, J.S., Skiniotis, G., and Kobilka, B.K. (2020). Structure of the neurotensin receptor 1 in complex with β-arrestin 1. Nature *579*, 303–308.

Iacovelli, L., Molinaro, G., Battaglia, G., Motolese, M., Di Menna, L., Alfiero, M., Blahos, J., Matrisciano, F., Corsi, M., Corti, C., et al. (2009). Regulation of group II metabotropic glutamate receptors by G protein-coupled receptor kinases: mGlu2 receptors are resistant to homologous desensitization. Mol. Pharmacol. *75*, 991–1003.

Iacovelli, L., Nicoletti, F., and De Blasi, A. (2013). Molecular mechanisms that desensitize metabotropic glutamate receptor signaling: an overview. Neuropharmacology *66*, 24–30.

Joffe, M.E., Santiago, C.I., Engers, J.L., Lindsley, C.W., and Conn, P.J. (2019). Metabotropic glutamate receptor subtype 3 gates acute stress-induced dysregulation of amygdalo-cortical function. Mol. Psychiatry *24*, 916–927.

Kang, Y., Zhou, X.E., Gao, X., He, Y., Liu, W., Ishchenko, A., Barty, A., White, T.A., Yefanov, O., Han, G.W., et al. (2015). Crystal structure of rhodopsin bound to arrestin by femtosecond X-ray laser. Nature *523*, 561–567.

Kawabata, S., Tsutsumi, R., Kohara, A., Yamaguchi, T., Nakanishi, S., and Okada, M. (1996). Control of calcium oscillations by phosphorylation of metabotropic glutamate receptors. Nature *383*, 89–92.

Kniazeff, J., Bessis, A.S., Maurel, D., Ansanay, H., Prézeau, L., and Pin, J.P. (2004). Closed state of both binding domains of homodimeric mGlu receptors is required for full activity. Nat. Struct. Mol. Biol. *11*, 706–713.

Kohout, T.A., Lin, F.S., Perry, S.J., Conner, D.A., and Lefkowitz, R.J. (2001). beta-Arrestin 1 and 2 differentially regulate heptahelical receptor signaling and trafficking. Proc. Natl. Acad. Sci. USA *98*, 1601–1606.

Komolov, K.E., and Benovic, J.L. (2018). G protein-coupled receptor kinases: Past, present and future. Cell. Signal. *41*, 17–24.

Komolov, K.E., Du, Y., Duc, N.M., Betz, R.M., Rodrigues, J.P.G.L.M., Leib, R.D., Patra, D., Skiniotis, G., Adams, C.M., Dror, R.O., et al. (2017). Structural and Functional Analysis of a β_2-Adrenergic Receptor Complex with GRK5. Cell *169*, 407–421.e16.

Kong, G., Penn, R., and Benovic, J.L. (1994). A beta-adrenergic receptor kinase dominant negative mutant attenuates desensitization of the beta 2-adrenergic receptor. J. Biol. Chem. *269*, 13084–13087.

Kumari, P., Srivastava, A., Banerjee, R., Ghosh, E., Gupta, P., Ranjan, R., Chen, X., Gupta, B., Gupta, C., Jaiman, D., and Shukla, A.K. (2016). Functional competence of a partially engaged GPCR-β-arrestin complex. Nat. Commun. *7*, 13416.

Latorraca, N.R., Wang, J.K., Bauer, B., Townshend, R.J.L., Hollingsworth, S.A., Olivieri, J.E., Xu, H.E., Sommer, M.E., and Dror, R.O. (2018). Molecular mechanism of GPCR-mediated arrestin activation. Nature *557*, 452–456.

Lee, M.H., Appleton, K.M., Strungs, E.G., Kwon, J.Y., Morinelli, T.A., Peterson, Y.K., Laporte, S.A., and Luttrell, L.M. (2016). The conformational signature of β-arrestin2 predicts its trafficking and signalling functions. Nature *531*, 665–668.

Lee, S., Park, S., Lee, H., Han, S., Song, J.M., Han, D., and Suh, Y.H. (2019). Nedd4 E3 ligase and beta-arrestins regulate ubiquitination, trafficking, and stability of the mGlu7 receptor. eLife *8*, e44502.

Lee, J., Munguba, H., Gutzeit, V.A., Singh, D.R., Kristt, M., Dittman, J.S., and Levitz, J. (2020). Defining the Homo- and Heterodimerization Propensities of Metabotropic Glutamate Receptors. Cell Rep. *31*, 107605.

Leff, E.R., Arttamangkul, S., and Williams, J.T. (2020). Chronic Treatment with Morphine Disrupts Acute Kinase-Dependent Desensitization of GPCRs. Mol. Pharmacol. *98*, 497–507.

Levitz, J., Habrian, C., Bharill, S., Fu, Z., Vafabakhsh, R., and Isacoff, E.Y. (2016). Mechanism of Assembly and Cooperativity of Homomeric and Heteromeric Metabotropic Glutamate Receptors. Neuron *92*, 143–159.

Lin, F.T., Krueger, K.M., Kendall, H.E., Daaka, Y., Fredericks, Z.L., Pitcher, J.A., and Lefkowitz, R.J. (1997). Clathrin-mediated endocytosis of the beta-adrenergic receptor is regulated by phosphorylation/dephosphorylation of beta-arrestin1. J. Biol. Chem. *272*, 31051–31057.

Lodowski, D.T., Pitcher, J.A., Capel, W.D., Lefkowitz, R.J., and Tesmer, J.J. (2003). Keeping G proteins at bay: a complex between G protein-coupled receptor kinase 2 and Gbetagamma. Science *300*, 1256–1262.

Logothetis, D.E., Kurachi, Y., Galper, J., Neer, E.J., and Clapham, D.E. (1987). The beta gamma subunits of GTP-binding proteins activate the muscarinic K+ channel in heart. Nature *325*, 321–326.

Luttrell, L.M., Wang, J., Plouffe, B., Smith, J.S., Yamani, L., Kaur, S., Jean-Charles, P.Y., Gauthier, C., Lee, M.H., Pani, B., et al. (2018). Manifold roles of β-arrestins in GPCR signaling elucidated with siRNA and CRISPR/Cas9. Sci. Signal. *11*, eaat7650.

Mangmool, S., and Kurose, H. (2011). G(i/o) protein-dependent and -independent actions of Pertussis Toxin (PTX). Toxins (Basel) *3*, 884–899.

Marchese, A., and Benovic, J.L. (2001). Agonist-promoted ubiquitination of the G protein-coupled receptor CXCR4 mediates lysosomal sorting. J. Biol. Chem. *276*, 45509–45512.

Maxfield, F.R., and McGraw, T.E. (2004). Endocytic recycling. Nat. Rev. Mol. Cell Biol. *5*, 121–132.

Ménard, L., Ferguson, S.S., Zhang, J., Lin, F.T., Lefkowitz, R.J., Caron, M.G., and Barak, L.S. (1997). Synergistic regulation of beta2-adrenergic receptor sequestration: intracellular complement of beta-adrenergic receptor kinase and beta-arrestin determine kinetics of internalization. Mol. Pharmacol. *51*, 800–808.

Miess, E., Gondin, A.B., Yousuf, A., Steinborn, R., Mösslein, N., Yang, Y., Göldner, M., Ruland, J.G., Bünemann, M., Krasel, C., et al. (2018). Multisite phosphorylation is required for sustained interaction with GRKs and arrestins during rapid μ-opioid receptor desensitization. Sci. Signal. *11*, eaas9609.

Mundell, S.J., Matharu, A.L., Pula, G., Roberts, P.J., and Kelly, E. (2001). Agonist-induced internalization of the metabotropic glutamate receptor 1a is arrestin- and dynamin-dependent. J. Neurochem. *78*, 546–551.

Neto, A., and Ceol, C.J. (2018). Melanoma-associated GRM3 variants dysregulate melanosome trafficking and cAMP signaling. Pigment Cell Melanoma Res. *31*, 115–119.

Nicoletti, F., Bockaert, J., Collingridge, G.L., Conn, P.J., Ferraguti, F., Schoepp, D.D., Wroblewski, J.T., and Pin, J.P. (2011). Metabotropic glutamate receptors: from the workbench to the bedside. Neuropharmacology *60*, 1017–1041.

Nobles, K.N., Xiao, K., Ahn, S., Shukla, A.K., Lam, C.M., Rajagopal, S., Strachan, R.T., Huang, T.Y., Bressler, E.A., Hara, M.R., et al. (2011). Distinct phosphorylation sites on the β(2)-adrenergic receptor establish a barcode that encodes differential functions of β-arrestin. Sci. Signal. *4*, ra51.

Nuber, S., Zabel, U., Lorenz, K., Nuber, A., Milligan, G., Tobin, A.B., Lohse, M.J., and Hoffmann, C. (2016). β-Arrestin biosensors reveal a rapid, receptor-dependent activation/deactivation cycle. Nature *531*, 661–664.

O'Hayre, M., Vázquez-Prado, J., Kufareva, I., Stawiski, E.W., Handel, T.M., Seshagiri, S., and Gutkind, J.S. (2013). The emerging mutational landscape of G proteins and G-protein-coupled receptors in cancer. Nat. Rev. Cancer *13*, 412–424.

O'Hayre, M., Eichel, K., Avino, S., Zhao, X., Steffen, D.J., Feng, X., Kawakami, K., Aoki, J., Messer, K., Sunahara, R., et al. (2017). Genetic evidence that β-arrestins are dispensable for the initiation of β_2-adrenergic receptor signaling to ERK. Sci. Signal. *10*, eaal3395.

Oakley, R.H., Laporte, S.A., Holt, J.A., Caron, M.G., and Barak, L.S. (2000). Differential affinities of visual arrestin, beta arrestin1, and beta arrestin2 for G protein-coupled receptors delineate two major classes of receptors. J. Biol. Chem. *275*, 17201–17210.

Peterson, Y.K., and Luttrell, L.M. (2017). The Diverse Roles of Arrestin Scaffolds in G Protein-Coupled Receptor Signaling. Pharmacol. Rev. *69*, 256–297.

Pitcher, J.A., Inglese, J., Higgins, J.B., Arriza, J.L., Casey, P.J., Kim, C., Benovic, J.L., Kwatra, M.M., Caron, M.G., and Lefkowitz, R.J. (1992). Role of beta gamma subunits of G proteins in targeting the beta-adrenergic receptor kinase to membrane-bound receptors. Science *257*, 1264–1267.

Prickett, T.D., Wei, X., Cardenas-Navia, I., Teer, J.K., Lin, J.C., Walia, V., Gartner, J., Jiang, J., Cherukuri, P.F., Molinolo, A., et al. (2011). Exon capture analysis of G protein-coupled receptors identifies activating mutations in GRM3 in melanoma. Nat. Genet. *43*, 1119–1126.

Rajagopal, S., and Shenoy, S.K. (2018). GPCR desensitization: Acute and prolonged phases. Cell. Signal. *41*, 9–16.

Raveh, A., Cooper, A., Guy-David, L., and Reuveny, E. (2010). Nonenzymatic rapid control of GIRK channel function by a G protein-coupled receptor kinase. Cell *143*, 750–760.

Reiner, A., and Levitz, J. (2018). Glutamatergic Signaling in the Central Nervous System: Ionotropic and Metabotropic Receptors in Concert. Neuron *98*, 1080–1098.

Ribeiro, F.M., Ferreira, L.T., Paquet, M., Cregan, T., Ding, Q., Gros, R., and Ferguson, S.S. (2009). Phosphorylation-independent regulation of metabotropic glutamate receptor 5 desensitization and internalization by G protein-coupled receptor kinase 2 in neurons. J. Biol. Chem. *284*, 23444–23453.

Saugstad, J.A., Segerson, T.P., and Westbrook, G.L. (1996). Metabotropic glutamate receptors activate G-protein-coupled inwardly rectifying potassium channels in Xenopus oocytes. J. Neurosci. *16*, 5979–5985.

Scheefhals, N., Catsburg, L.A.E., Westerveld, M.L., Blanpied, T.A., Hoogenraad, C.C., and MacGillavry, H.D. (2019). Shank Proteins Couple the Endocytic Zone to the Postsynaptic Density to Control Trafficking and Signaling of Metabotropic Glutamate Receptor 5. Cell Rep. *29*, 258–269.e8.

Schindelin, J., Arganda-Carreras, I., Frise, E., Kaynig, V., Longair, M., Pietzsch, T., Preibisch, S., Rueden, C., Saalfeld, S., Schmid, B., et al. (2012). Fiji: an open-source platform for biological-image analysis. Nat. Methods *9*, 676–682.

Schneider, C.A., Rasband, W.S., and Eliceiri, K.W. (2012). NIH Image to ImageJ: 25 years of image analysis. Nat. Methods *9*, 671–675.

Sente, A., Peer, R., Srivastava, A., Baidya, M., Lesk, A.M., Balaji, S., Shukla, A.K., Babu, M.M., and Flock, T. (2018). Molecular mechanism of modulating arrestin conformation by GPCR phosphorylation. Nat. Struct. Mol. Biol. *25*, 538–545.

Shenoy, S.K., and Lefkowitz, R.J. (2011). β-Arrestin-mediated receptor trafficking and signal transduction. Trends Pharmacol. Sci. *32*, 521–533.

Shenoy, S.K., McDonald, P.H., Kohout, T.A., and Lefkowitz, R.J. (2001). Regulation of receptor fate by ubiquitination of activated beta 2-adrenergic receptor and beta-arrestin. Science *294*, 1307–1313.

Shukla, A.K., Westfield, G.H., Xiao, K., Reis, R.I., Huang, L.Y., Tripathi-Shukla, P., Qian, J., Li, S., Blanc, A., Oleskie, A.N., et al. (2014). Visualization of arrestin recruitment by a G-protein-coupled receptor. Nature *512*, 218–222.

Sorensen, S.D., and Conn, P.J. (2003). G protein-coupled receptor kinases regulate metabotropic glutamate receptor 5 function and expression. Neuropharmacology *44*, 699–706.

Stauffer, W., Sheng, H., and Lim, H.N. (2018). EzColocalization: An ImageJ plugin for visualizing and measuring colocalization in cells and organisms. Sci. Rep. *8*, 15764.

Staus, D.P., Hu, H., Robertson, M.J., Kleinhenz, A.L.W., Wingler, L.M., Capel, W.D., Latorraca, N.R., Lefkowitz, R.J., and Skiniotis, G. (2020). Structure of the M2 muscarinic receptor-β-arrestin complex in a lipid nanodisc. Nature *579*, 297–302.

Stoeber, M., Jullié, D., Li, J., Chakraborty, S., Majumdar, S., Lambert, N.A., Manglik, A., and von Zastrow, M. (2020). Agonist-selective recruitment of engineered protein probes and of GRK2 by opioid receptors in living cells. eLife *9*, e54208.

Stoppel, L.J., Auerbach, B.D., Senter, R.K., Preza, A.R., Lefkowitz, R.J., and Bear, M.F. (2017). β-Arrestin2 Couples Metabotropic Glutamate Receptor 5 to Neuronal Protein Synthesis and Is a Potential Target to Treat Fragile X. Cell Rep. *18*, 2807–2814.

Subtil, A., Lampson, M.A., Keller, S.R., and McGraw, T.E. (2000). Characterization of the insulin-regulated endocytic recycling mechanism in 3T3-L1 adipocytes using a novel reporter molecule. J. Biol. Chem. *275*, 4787–4795.

Suh, Y.H., Chang, K., and Roche, K.W. (2018). Metabotropic glutamate receptor trafficking. Mol. Cell. Neurosci. *91*, 10–24.

Tesmer, V.M., Kawano, T., Shankaranarayanan, A., Kozasa, T., and Tesmer, J.J. (2005). Snapshot of activated G proteins at the membrane: the Galphaq-GRK2-Gbetagamma complex. Science *310*, 1686–1690.

Tora, A.S., Rovira, X., Cao, A.M., Cabayé, A., Olofsson, L., Malhaire, F., Scholler, P., Baik, H., Van Eeckhaut, A., Smolders, I., et al. (2018). Chloride ions stabilize the glutamate-induced active state of the metabotropic glutamate receptor 3. Neuropharmacology *140*, 275–286.

Vafabakhsh, R., Levitz, J., and Isacoff, E.Y. (2015). Conformational dynamics of a class C G-protein-coupled receptor. Nature *524*, 497–501.

Violin, J.D., Dewire, S.M., Barnes, W.G., and Lefkowitz, R.J. (2006). G protein-coupled receptor kinase and beta-arrestin-mediated desensitization of the angiotensin II type 1A receptor elucidated by diacylglycerol dynamics. J. Biol. Chem. *281*, 36411–36419.

Vivaudou, M., Chan, K.W., Sui, J.L., Jan, L.Y., Reuveny, E., and Logothetis, D.E. (1997). Probing the G-protein regulation of GIRK1 and GIRK4, the two subunits of the KACh channel, using functional homomeric mutants. J. Biol. Chem. *272*, 31553–31560.

von Zastrow, M., and Kobilka, B.K. (1992). Ligand-regulated internalization and recycling of human beta 2-adrenergic receptors between the plasma membrane and endosomes containing transferrin receptors. J. Biol. Chem. *267*, 3530–3538.

Whorton, M.R., and MacKinnon, R. (2013). X-ray structure of the mammalian GIRK2-βγ G-protein complex. Nature *498*, 190–197.

Yanagawa, M., Hiroshima, M., Togashi, Y., Abe, M., Yamashita, T., Shichida, Y., Murata, M., Ueda, M., and Sako, Y. (2018). Single-molecule diffusion-based estimation of ligand effects on G protein-coupled receptors. Sci. Signal. *11*, eaao1917.

Zhao, Y., Araki, S., Wu, J., Teramoto, T., Chang, Y.F., Nakano, M., Abdelfattah, A.S., Fujiwara, M., Ishihara, T., Nagai, T., and Campbell, R.E. (2011). An expanded palette of genetically encoded Ca^{2+} indicators. Science *333*, 1888–1891.

Zhou, X.E., He, Y., de Waal, P.W., Gao, X., Kang, Y., Van Eps, N., Yin, Y., Pal, K., Goswami, D., White, T.A., et al. (2017). Identification of Phosphorylation Codes for Arrestin Recruitment by G Protein-Coupled Receptors. Cell *170*, 457–469.e13.

STAR★METHODS

KEY RESOURCES TABLE

REAGENT or RESOURCE	SOURCE	IDENTIFIER
Chemicals, peptides, and recombinant proteins		
Dulbecco's Modified Eagle Medium (DMEM)	Thermo Fisher Scientific	Cat#11995073
Fetal Bovine Serum (FBS)	Thermo Fisher Scientific	Cat#10437028
SNAP-Surface Alexa Fluor 546 (BG-Alexa 546)	New England Biolabs	Cat#S9132S
SNAP-Surface Alexa Fluor 488 (BG-Alexa 488)	New England Biolabs	Cat#S9232S
Lipofectamine 2000 Transfection Reagent	Thermo Fisher Scientific	Cat#11668019
Lipofectamine 3000 Transfection Reagent	Thermo Fisher Scientific	Ca#L300015
Poly-L-lysine (PLL) hydrobromide	Sigma Aldrich	Cat#P2636
Cy3-Transferrin (CY3-Tf)	Subtil et al., 2000	N/A
ML289	Tocris	Cat#4976
CMPD101	Tocris	Cat#5642
LY341495	Tocris	Cat#1209
Experimental models: Cell lines		
HEK293T	ATCC	Cat#CRL-11268; RRID:CVCL_1926
HEK293	ATCC	Cat#CRL-1573; RRID:CVCL_0045
HAR-HEK293 β-Arrestin1/2 KO Cell Lines	Luttrell et al., 2018	N/A
Recombinant DNA		
SNAP-tagged mGluRs	Doumazane et al., 2011	N/A
SNAP-β_2AR	Addgene	Cat#101123
GIRK1-F137S	Vivaudou et al., 1997	N/A
R-GECO	Zhao et al., 2011	N/A
β-arrestin1-YFP	Addgene	Cat#36916
β-arrestin2-YFP	Addgene	Cat#36917
β-arrestin2-RFP	Ahn et al., 2004	N/A
GRK2-GFP	Raveh et al., 2010	N/A
GFP-2xFYVE	Gillooly et al., 2000	N/A
mCherry-TGN38 (mCh-TGN38)	Addgene	Cat#55145
LAMP1-YFP	Addgene	Cat#1816
PTX-S1	Raveh et al., 2010	N/A
CLC-mCherry (CLC-mCh)	Addgene	Cat#27680
Software and algorithms		
ImageJ (Fiji)	Schneider et al., 2012	RRID:SCR_003070
Microsoft Excel	Microsoft Office	RRID:SCR_016137
Adobe Illustrator	Adobe	RRID:SCR_010279
Prism	GraphPad	RRID:SCR_002798
pCLAMP (Clampfit)	Molecular Devices	RRID:SCR_011323

RESOURCE AVAILABILITY

Lead contact

Further information and requests for resources and reagents should be directed to and will be fulfilled by the Lead Contact, Joshua Levitz (jtl2003@med.cornell.edu).

Materials availability

Requests for resources and reagents will be fulfilled by the Lead Contact with a completed Materials Transfer Agreement.

Data and code availability

This study did not generate large datasets or code. The datasets analyzed during the study are available from the corresponding author on reasonable request.

EXPERIMENTAL MODEL AND SUBJECT DETAILS

HEK293, HEK293T, parental and HAR CRISPR β-Arr1/2 KO cells (Luttrell et al., 2018) were cultured in DMEM (Fisher Scientific) supplemented with 5%–10% FBS and maintained at 37°C in a 5% CO_2 humidified incubator. HEK293 and 293T were obtained from ATCC and tested negative for mycoplasma contamination using a kit (Molecular Probes).

METHOD DETAILS

Molecular biology

Point mutations were made using site-directed mutagenesis. CTD or ST-rich region chimeras were made using a Gibson Assembly Cloning Kit (New England BioLabs). mGluR2-ΔCTD (Δaa821-872) and mGluR3-ΔCTD (Δaa830-879) were generated by introducing a premature stop codon at P821 and P830, respectively. ST chimeras and mGluR3-ΔST (Δaa841-860) were made utilizing a PCR-based DNA ligation method using primers with 5′ phosphates and the enzyme T4 DNA Ligase (Invitrogen).

Cell culture and transfection

Cells were seeded on poly-L-lysine-coated 18 mm coverslips and transfected ~18 hr later with either Lipofectamine 2000 or 3000 (Invitrogen). Cells were maintained in 5-10 μM LY341495 post-transfection to maintain cell health. All experiments were done at least 24 hours post-transfection unless otherwise stated.

Surface labeling assay

For the surface labeling assay, HEK293T cells transfected with 0.35 μg SNAP-tagged receptors (with or without 0.7 μg of the PTX-S1 subunit, YFP-tagged β-arr, or GFP-tagged GRK) were incubated in either no glutamate (media or 20 μM LY34) or 1 mM Glu (10 mM for mGluR7; 10 μM isoproterenol for β_2AR) in media for 60 min. To label remaining surface receptors, the cells were incubated in 1 μM BG-Alexa-546 (New England BioLabs) for 20 min at room temperature in an extracellular (EX) solution composed of (in mM) 135 NaCl, 5.4 KCl, 10 HEPES, 5 L-Glucose, 2 $CaCl_2$, and 1 $MgCl_2$ (pH 7.4). To block GRK2/3 kinase activity, cells were pre-incubated in 30 μM cmpd101 for 20 min. Following fluorophore labeling, live cells were washed and imaged on an inverted microscopy (Olympus IX83) with a 60x 1.49 NA objective. Alexa-546 was excited using a 560 nm laser and snapshots were acquired to measure the mean fluorescence intensity of labeled surface receptors using ImageJ. Fluorescence was normalized to the average fluorescence of the control. The raw fluorescence values were normalized to 20 uM LY34 rather than zero glutamate as a control in Figures 2 and 7. The decrease in surface fluorescence was calculated as 100 * (1-normalized surface fluorescence).

Internalization and arrestin recruitment assays

To observe the internalization of SNAP-tagged surface receptors, cells were incubated in 1 μM BG-Alexa-546 for 30-45 min at 37°C in extracellular solution. To induce internalization of SNAP-tagged receptors, cells were incubated with agonist in EX solution for 30 min at 37°C and imaged. mGluR7 was stimulated with 10 mM glutamate due to its low affinity, while other mGluRs were stimulated with 1 mM glutamate, Alexa-546 was excited with a 560 nm laser and snapshots of randomized fields were acquired. To block internalization of SNAP-mGluR3, cells were preincubated in 20 μM LY34 or 100 μM ML289 for 10-15 min, and the drugs were maintained during the glutamate incubation that followed. The basal condition was always run side-by-side with other conditions with the same allotted time but in EX solution that did not contain drugs.

For the β-arr recruitment experiments, HEK293T cells were co-transfected with 0.5-0.7 μg SNAP-mGluR2 or SNAP-mGluR3 and either 0.1-0.3 μg β-arr1-YFP or β-arr2-YFP. Since the expression levels of mGluR2 and mGluR3 differ at 24 hr, we expression-matched conditions by measuring arrestin-recruitment of mGluR2-CTD and -ST variants at 48 hr expression. For time lapse experiments, internalization of Alexa 546-labeled SNAP-mGluR and β-arr surface recruitment was followed on the microscope following bath application of 1 mM glutamate. Cells were maintained at 37°C using a temperature control device (TC-326C, Warner Instruments). For simple surface recruitment of β-arr experiments to quantify the percentage of cells with recruitment, cells were incubated in 1 mM glutamate for 15 min at room temperature and snapshots of the 488 channel were taken of randomized fields of cells.

The percentage of cells with internalization or β-arr recruitment was manually counted following blinding to the conditions. Internalization was defined by cells that exhibit clear intracellular accumulation of fluorescence. β-arr recruitment was defined by cells that exhibited higher YFP intensity on the cell surface compared with the inside. Cell-to-cell variability is also present and can likely be attributed to transient transfection of variable amounts of receptor and varying expression patterns of endogenous regulatory proteins. Values for % cells with internalization or β-arr recruitment are compared on the same days within the same

bar graph, with at least two separate days for each condition, as there is modest day-to-day variability that can confound results. This day-to-day variability explains the ~10%–15% fluctuation of some values for common conditions between figures.

Recycling assay

After 48 hr expression, HEK293T cells seeded on 12 mm coverslips transfected with ~0.2 μg SNAP-mGluR2 or SNAP-mGluR3 were incubated in 1 mM glutamate in complete media for 30 min at 37°C to internalize a population of receptors. Cells were then washed and labeled with 5 μM BG-Alexa 488 for 20 minutes at room temperature to label and occupy the SNAP-tag on all remaining surface receptors. Cells were then washed and incubated in media for either 30, 60, or 90 min to allow internalized receptors to recycle back to the surface. Following incubation, cells were then washed with media and labeled in 5 μM Alexa 546 for 20 min at room temperature to label receptors that trafficked back to the surface. Control coverslips did not receive a 30 min glutamate treatment. For all conditions, cells were maintained in 10 μM LY341495 when not treated with glutamate to avoid any confounding effects from ambient glutamate. Cells were washed in PBS and fixed in a 4% PFA/4% sucrose solution and coverslips were mounted on slides for imaging. Fixed cells were imaged with the 60x 1.49 NA objective. Alexa 488 and Alexa-546 were excited with 488 nm and 560 nm lasers respectively. For surface fluorescence analysis, mean intensity of ROIs draw around receptor-positive cells (based on the 488 channel) were measured on ImageJ. All raw fluorescence values were normalized to the BG-Alexa-546 fluorescence observed prior to post-glutamate incubation.

Confocal microscopy

To measure colocalization with the ERC, HEK293T cells expressing SNAP-mGluR3 or SNAP-mGluR2 were incubated in 1 μM BG-Alexa 488 in EX solution for ~45 min at 37°C followed by 5 μg/ml Cy3-transferrin + 1 mM glutamate in EX solution for 30 min at 37°C and fixed in a solution of 4% PFA/4% Sucrose. To measure colocalization of mGluR3 with lysosomes and TGN, cells expressing either SNAP-mGluR3 and LAMP1-YFP or mCh-TGN38, respectively, were incubated in 1 mM glutamate in EX solution for 30 min at 37°C and fixed. Cells were imaged using a 63x objective with 1.2x zoom on a Zeiss LSM880 scanning confocal microscope and the ZEN Black software. Fluorophores were excited using 488 nm and/or 561 nm lasers. The plane of imaging was chosen based on the organelle marker channel. Images were captured using one directional scanning and a pinhole of 1 Airy unit. For the image analysis, region of interests (ROIs) were drawn within the cells to exclude the surface receptors. The pixels with the top 10% highest intensity (F_T) in each channel was used to measure the Pearson's correlation coefficient (PCC) via the plugin EzColocalization (Stauffer et al., 2018) on ImageJ.

Total internal reflection fluorescence microscopy

HEK293T cells were seeded sparsely and transfected with 0.5-0.7 μg SNAP-tagged receptors with or without 0.1-0.3 μg GFP-2xFYVE, β-arr1-YFP, β-arr2-YFP, β-arr2-RFP, or CLC-mCh. SNAP-tags were labeled with BG-Alexa 546 or 488 and then maintained at 37°C on the microscope. Agonist was applied by bath application and images were captured with a 100x 1.49 NA Apo N objective in TIRF mode after ~15 min. Receptor and β-arr puncta were manually counted using the multi-point tool on ImageJ. To determine colocalization and overlap of puncta, the puncta of one channel were marked in the center with the multi-point tool. The markers denoting the location of puncta from one channel was transferred to the next channel to determine the number of puncta that contained a marker in its center. These puncta were counted as overlapping.

Patch clamp electrophysiology

HEK293T cells were transfected with 0.35-0.7 μg SNAP-tagged mGluRs, GIRK1-F137S homotetramerization mutant (Vivaudou et al., 1997), tdTomato (as a transfection marker), with or without WT or mutant 0.35 μg (1x) or 0.7 μg (2x) GRK2-GFP, or 0.7 μg each of β-arr1-YFP and β-arr2-YFP. Whole-cell patch clamp experiments were performed 24-36 hr after transfection in a high potassium extracellular solution composed of (in mM) 120 KCl, 25 NaCl, 10 HEPES, 2 $CaCl_2$, and 1 $MgCl_2$ (pH 7.4). Solutions were delivered to a recording chamber using a gravity-driven perfusion system with exchange times of ~1 s. Cells were voltage-clamped at −60 mV using an Axopatch 200B amplifier (Molecular Devices). Patch pipettes with resistances of 4-10 MΩ were filled with an intracellular solution composed of (in mM): 140 KCl, 10 HEPES, 3 Na_2ATP, 0.2 Na_2GTP, 5 EGTA, 3 $MgCl_2$ (pH 7.4). Inward GIRK currents were induced with the perfusion of glutamate. Desensitization of currents were measured over 30-60 s glutamate application (40 s for mGluR7, 60 s for mGluR3-ΔCTD, 30 s for all other receptors). For the repeated glutamate application experiment, 100 μM glutamate was applied for ~1 min and washed out for ~1 min before reapplying glutamate. Currents were sampled at 10 kHz and filtered using a low-pass Bessel (8-pole) at 2 kHz.

Recordings were analyzed using Clampfit (Molecular Devices) and Prism (GraphPad) software. Calculation of glutamate-dependent current amplitudes were quantified relative to the average baseline amplitude. Desensitization of the glutamate-induced responses was calculated over 30 s or 60 s as follows: 100* (1 – (amplitude prior to glutamate washout) / (peak amplitude following glutamate application)). Comparisons were done on the same and across multiple days to account for variability. Percent increase in desensitization (Figures 3F, 3I, 5F, and 6F) was calculated as: 100* ((mean desensitization of currents) – (mean desensitization of control currents)) / (mean desensitization of control currents). The mean desensitization of currents was averaged from the same experimental day. The standard error of the mean (s.e.m.) was calculated from the average of multiple experimental days. The tau of desensitization was calculated from the peak amplitude to glutamate washout, fit to a single exponential curve in Clampfit.

Calcium imaging

HEK293T cells were transfected with the calcium indicator, 0.2 μg R-GECO (Zhao et al., 2011), and 0.4-0.7 μg SNAP-mGluR1 or SNAP-mGluR5, with or without 0.4 μg WT or mutant GRK2-GFP, were imaged on an inverted microscope (Olympus IX83) with a 20x objective at room temperature in EX solution with continuous perfusion following 24 hr expression. R-GECO was excited using a 561 nm laser at 0.5 Hz with a 100 ms exposure time. Receptors were activated with a perfusion of 100 μM glutamate. Time-lapse movies were recorded with an scMOS camera (Hamamatsu ORCA-Flash4v3.0). Image analysis was performed using ImageJ (Fiji) (Schindelin et al., 2012). Intensities were normalized to baseline prior to glutamate application. Full width at half maximum (FWHM) was calculated as the width (duration of time, measured in seconds) of an average trace (40-60 cells) representing the calcium transient achieved after glutamate application measured at half of its maximum amplitude. Peak amplitude was determined as the highest value of arbitrary unit fluorescence reached after glutamate application.

QUANTIFICATION AND STATISTICAL ANALYSIS

Statistics were calculated using GraphPad Prism. Only two-tailed t tests were performed unless otherwise stated, and pairing is specified in the figure legends. Data is represented as mean ± s.e.m. and averaged across multiple independent experiments.

Cell Reports, Volume *35*

Supplemental information

Mechanisms of differential desensitization of metabotropic glutamate receptors

Nohely Abreu, Amanda Acosta-Ruiz, Guoqing Xiang, and Joshua Levitz

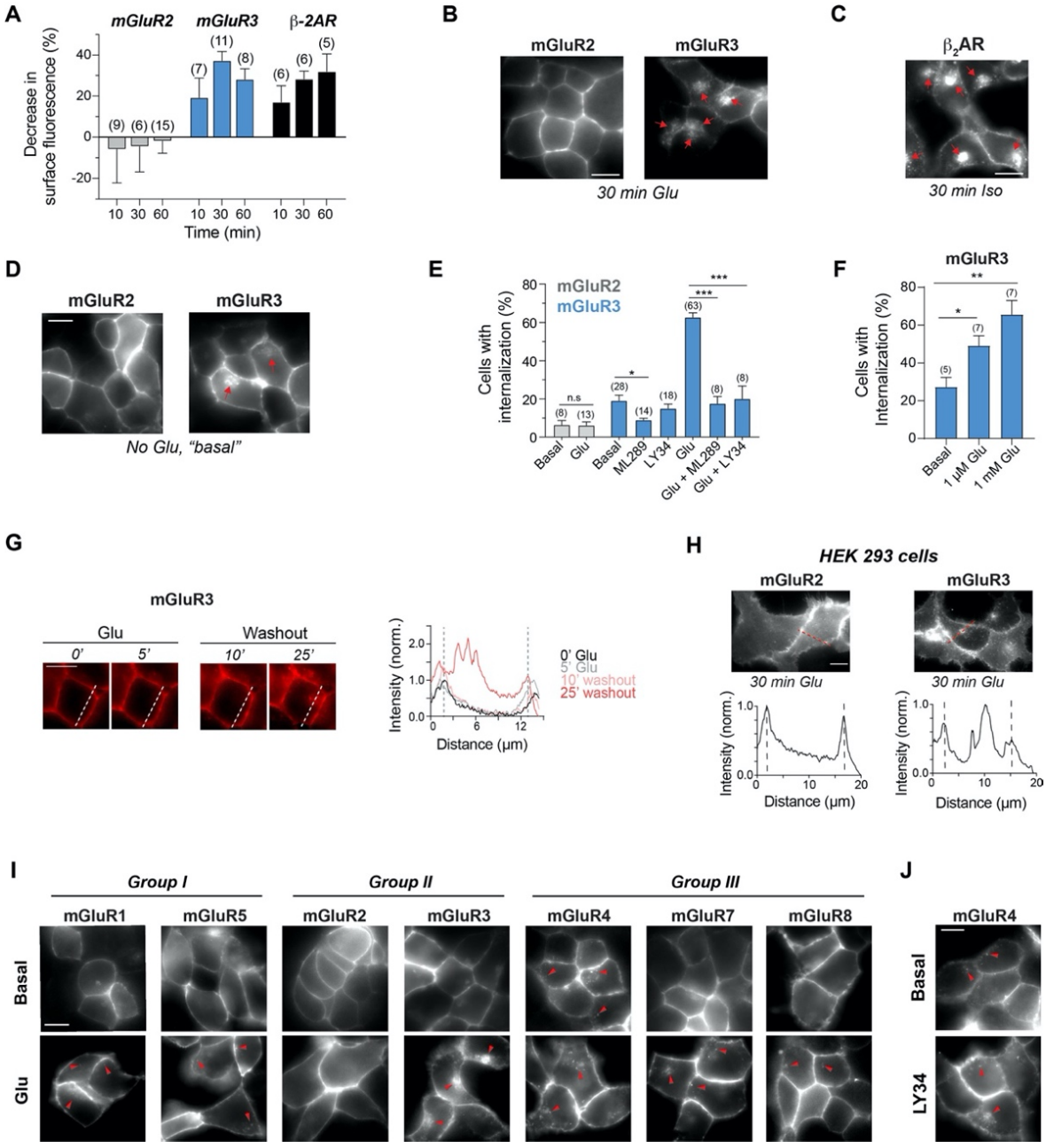

Figure S1. Further analysis of mGluR internalization, Related to Figure 1

(A) HEK 293T cells expressing BG-546-labeled SNAP-mGluR2, -mGluR3, or -β_2AR were stimulated with 1 mM Glu (mGluR) or 10 μM Iso (β_2AR) for the indicated times to measure the percent decrease in surface fluorescence as compared to no agonist control.

(B-C) Representative images of HEK 293T cells expressing either BG-546-labeled mGluR2, mGluR3 (B), or β_2AR (C) following 30 min of agonist treatment. Red arrows point to internalized receptors. Scale bar=10 μm.

(D) Images showing that under basal conditions, mGluR3 but not mGluR2 can internalize. Red arrows point to internalized mGluR3.

(E) Summary bar graph of the percentage of cells that exhibit internalization of either mGluR2 or mGluR3. ML289 partially blocks the basal internalization of mGluR3, and both 100 μM ML289 and 20 μM LY34 block glutamate-mediated internalization of mGluR3. * indicates statistical significance (unpaired t-tests, p= 0.02 for Basal vs ML289, <0.0001 for Glu vs Glu + ML289, and <0.0001 for Glu vs Glu + LY34).
(F) Quantification of the percentage of cells that exhibit mGluR3 internalization following 30 min of either 1 μM or 1 mM glutamate treatment. * indicates statistical significance (unpaired t-tests, p=0.02 for 1 μM, 0.003 for 1 mM).
(G) Left, time-lapse images of a HEK 293T cell expressing BG-546-labeled SNAP-mGluR3. After 5 min in 1 mM glutamate, cells were washed continuously for 25 min. Right, intensity line scan through the white dotted line on the images showing that after 25 min washout (red line), there is clear mGluR3 fluorescence inside the cell. Black dotted lines represent the cell surface.
(H) Top, Representative images of HEK 293 cells showing that mGluR3 but not mGluR2 can internalize in this cell type after 30 min 1 mM glutamate treatment. Bottom, intensity line scans taken from the red dotted lines on the images. The black dotted lines represent the cell surface.
(I) Representative images of BG-546-labeled mGluRs in HEK 293T cells under basal conditions and after 30 min glutamate treatment. Red arrows point to internalized receptors.
(J) Representative images of BG-546-labeled mGluR4 in HEK 293T cells under basal conditions and 45 min treatment with 20 μm LY34 during BG-546 labeling. Red arrows point to internalized receptors.
The number of fields of cells used in the analysis are in parentheses. Scale bars=10 μm. Error bars show s.e.m.

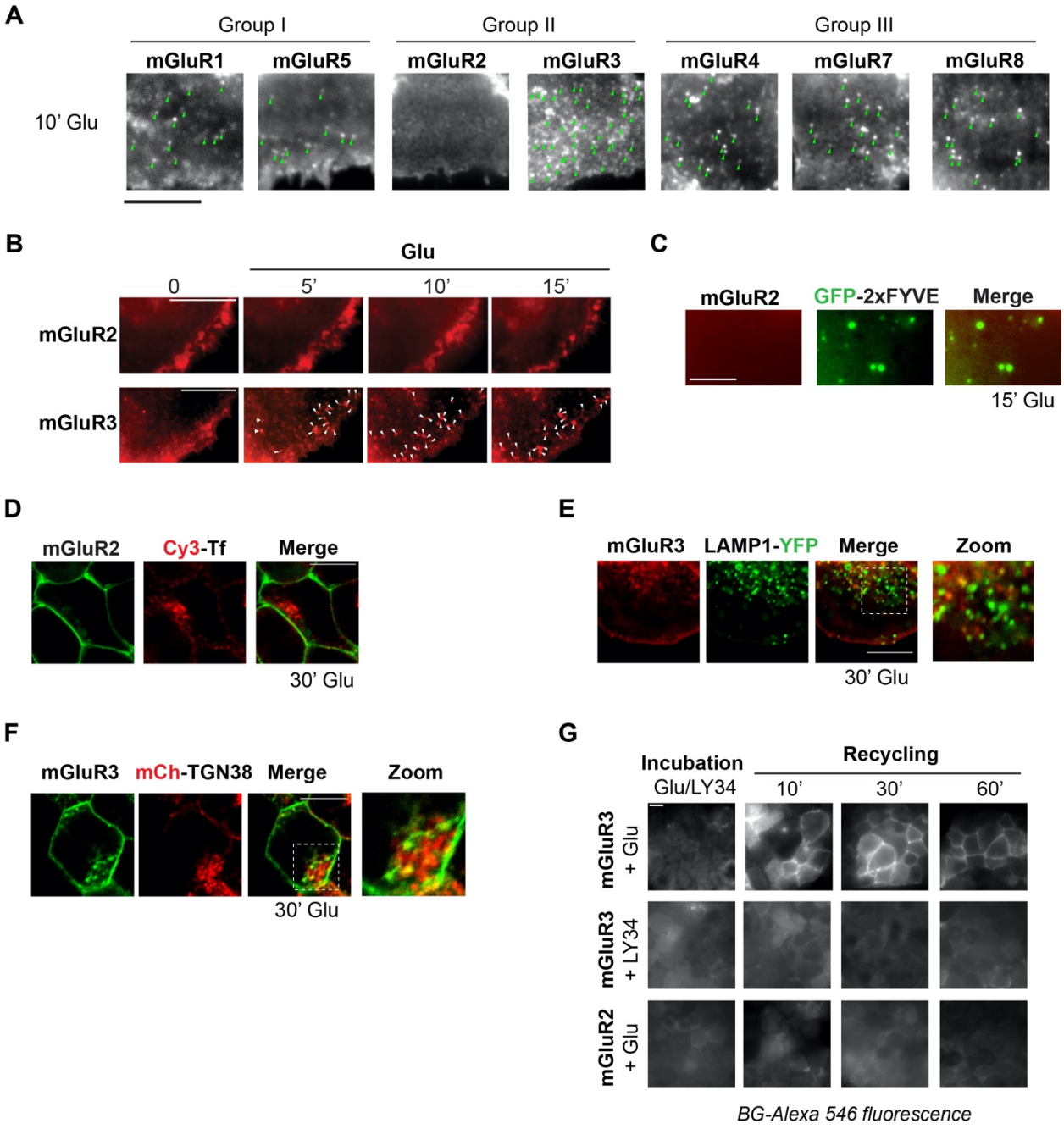

Figure S2. Further characterization of the sub-cellular localization of mGluRs, Related to Figure 1
(A) TIRF images of BG-Alexa546-labeled SNAP-mGluRs in HEK 293T cells following 10 min glutamate treatment. Green arrows highlight examples of receptor puncta. Scale bar= 5 µm.
(B) Time-lapse TIRF images of HEK 293T cells showing that after 5 min treatment in 1 mM glutamate, new mGluR3 puncta emerge and continue to emerge for 15 min. White arrowheads mark newly formed puncta. Scale bar= 10 µm.
(C) TIRF image showing the absence of mGluR2 puncta at GFP-2xFYVE puncta following 15 min glutamate treatment. Scale bar= 5 µm.

(D-F) Confocal images of cells showing a lack of colocalization between BG-488-labeled mGluR2 and Cy3-Tf (D), BG-546-labeled mGluR3 and LAMP1-YFP (E), and BG-488-labeled mGluR3 and mCherry-TGN38 (F) following 30 min in glutamate.
(G) Representative images from the recycling assay. mGluR3-expressing cells, following 30 min in 1 mM glutamate and not 10 μM LY34, show a gain of surface fluorescence following labeling with BG-546 after 10, 30, or 60 min of recycling. mGluR2 does not show surface labeling following incubation in glutamate. Scale bar= 10 μm.

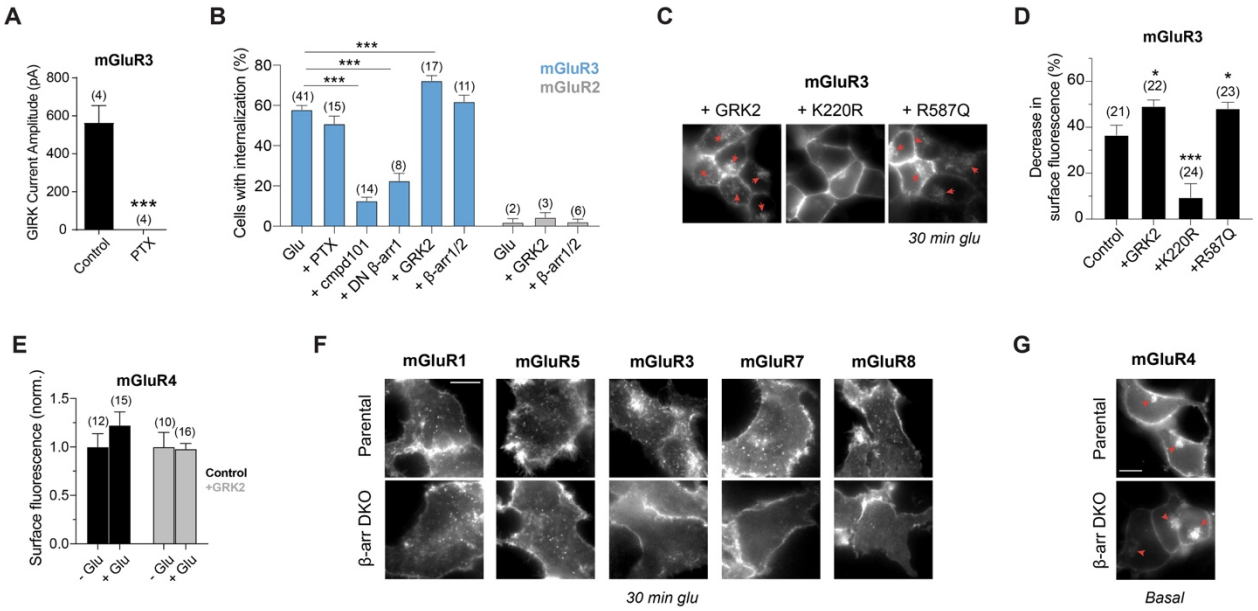

Figure S3. Further characterization of GRK and arrestin dependence of mGluR internalization, Related to Figure 2

(A) Quantification of the amplitudes of mGluR3-mediated GIRK currents following 100 μM glutamate application, without (control) and with co-expression of PTX. *** indicates statistical significance (unpaired t-test, p=0.0008). Number of cells recorded from are shown in parentheses.

(B) Summary bar graph of the percentage of cells that exhibit glutamate-dependent internalization of mGluR3 or mGluR2, with co-expression of either PTX, DN β-arr1, GRK2, GRK2-K220R, GRK2-R587Q, β-arrestin1 and β-arrestin2, or treatment with cmpd101. *** indicates statistical significance (unpaired t-test, p<0.0001 for cmpd101, p<0.0001 for DN β-arr1, p=0.0002 for GRK2). Number of fields of cells analyzed are in parentheses.

(C) Representative images of BG-546-labeled mGluR3 following incubation in 1 mM Glu for 30 min, with overexpression of either GRK2, GRK2-K220R, or GRK2-R587Q. Red arrows point at internalized receptors.

(D) Quantification of BG-Alexa-546-labeled mGluR3 fluorescence following incubation in 1 mM Glu for 60 min, with overexpression of either GRK2, GRK2-K220R, or GRK2-R587Q. Unpaired t tests compared to Glu, * p=0.01 for GRK2, *** p=0.0009 for K220R, * p= 0.03 for R587Q. Number of fields of cells analyzed are in parentheses.

(E) Quantification of BG-Alexa-546-labeled mGluR4 fluorescence before and after 60 min 1 mM Glu treatment, with and without overexpression of GRK2. Data is normalized to -Glu in the respective condition. Number of fields of cells analyzed are in parentheses.

(F) Images of BG-546-labeled mGluRs in CRISPR β-arrestin DKO and parental cells following incubation in Glu for 30 min.

(G) Representative images of BG-546-labeled mGluR4 under basal conditions in CRISPR β-arr DKO and parental cells. Red arrows point at internalized receptors.

Scale bars= 10 μm. Error bars show s.e.m.

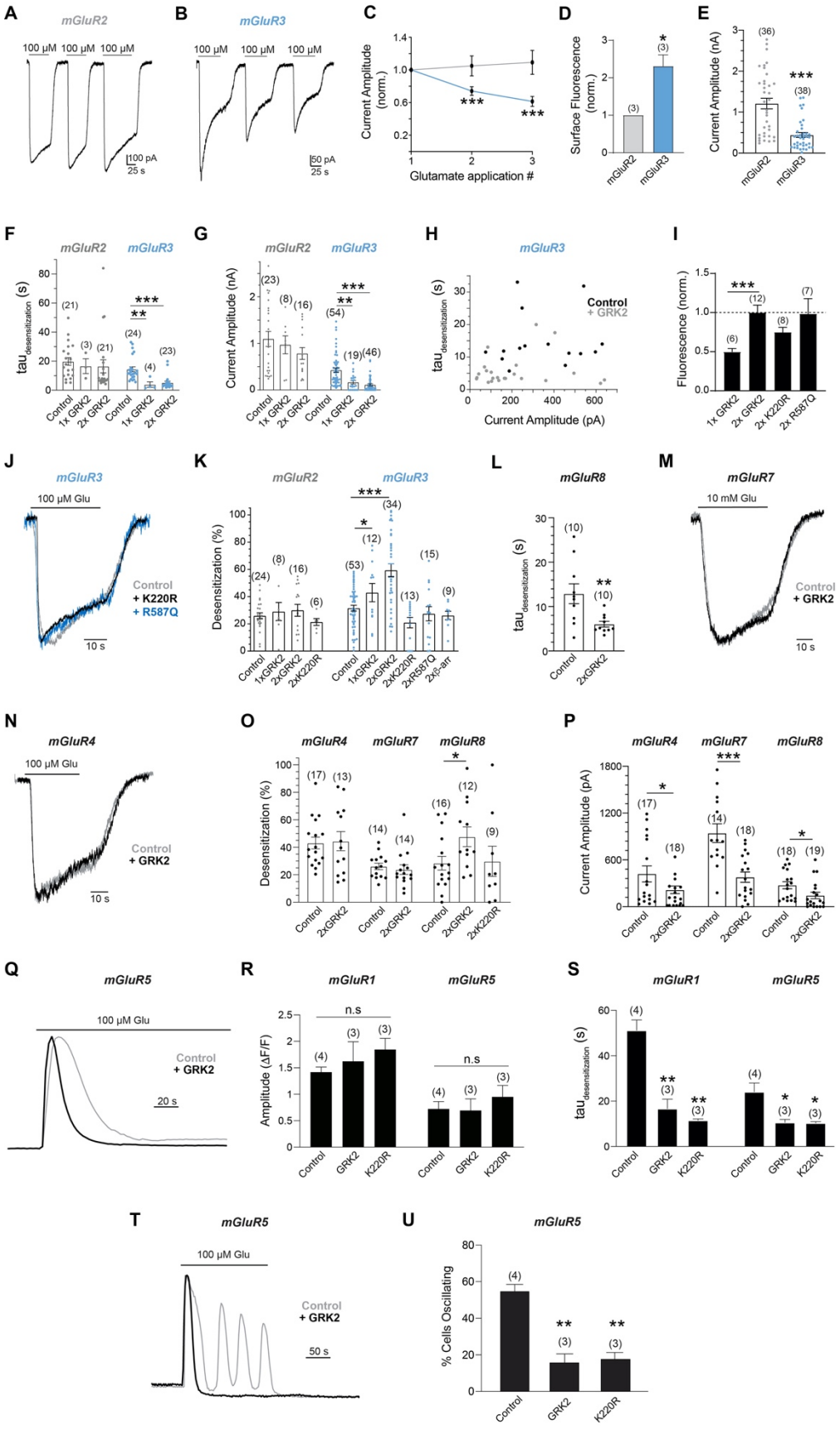
A
mGluR2
100 µM 100 µM 100 µM
100 pA
25 s
B
mGluR3
100 µM 100 µM 100 µM
50 pA
25 s
C
Current Amplitude (norm.)
Glutamate application #
D
Surface Fluorescence (norm.)
mGluR2
mGluR3
E
Current Amplitude (nA)
F
tau desensitization (s)
Control
1x GRK2
2x GRK2
G
Current Amplitude (nA)
H
tau desensitization (s)
Control
+ GRK2
Current Amplitude (pA)
I
Fluorescence (norm.)
1x GRK2
2x GRK2
2x K220R
2x R587Q
J
mGluR3
100 µM Glu
Control
+ K220R
+ R587Q
10 s
K
Desensitization (%)
Control
1xGRK2
2xGRK2
2xK220R
2xR587Q
2xβ-arr
L
mGluR8
tau desensitization (s)
Control
2xGRK2
M
mGluR7
10 mM Glu
Control
+ GRK2
10 s
N
mGluR4
100 µM Glu
Control
+ GRK2
10 s
O
mGluR4
mGluR7
mGluR8
Desensitization (%)
Control
2xGRK2
2xK220R
P
mGluR4
mGluR7
mGluR8
Current Amplitude (pA)
Q
mGluR5
100 µM Glu
Control
+ GRK2
20 s
R
mGluR1
mGluR5
Amplitude (ΔF/F)
n.s
Control
GRK2
K220R
S
mGluR1
mGluR5
tau desensitization (s)
T
mGluR5
100 µM Glu
Control
+ GRK2
50 s
U
mGluR5
% Cells Oscillating
Control
GRK2
K220R

Figure S4. Further analysis of GRK-mediated rapid desensitization of mGluR signaling, Related to Figure 3

(A-B) Representative whole cell patch clamp recordings in HEK 293T cells of GIRK currents following repeated 1 min activation of mGluR2 (A) or mGluR3 (B) by glutamate.

(C) Summary plot showing that repeated glutamate applications reduce the peak amplitudes of mGluR3-mediated currents, but not mGluR2. Values are normalized to the average amplitude of the 1st glutamate application for each receptor. Measurements were taken from individual cells, n=5 for mGluR3, n=12 for mGluR2. Repeated measures one-way ANOVA, *** p=0.0006.

(D) Quantification of the surface fluorescence of BG-546-labeled mGluR2 and mGluR3 in HEK 293T cells following 24 hr expression. Fluorescence is normalized to the average value of mGluR2. Number of independent experiments are in parentheses. Unpaired t-test, * p=0.01.

(E) Quantification of the average GIRK current amplitudes mediated by either mGluR2 or mGluR3. Activation was induced with 100 μM glutamate. Unpaired t-test, *** p<0.0001.

(F) Summary bar graph comparing the tau of desensitization of GIRK currents mediated by mGluR2 or mGluR3 during 30 s 100 μm glutamate application. Unpaired t-tests compared to mGluR3 control, * p=0.02 for 1xGRK2, *** p<0.0001 for 2xGRK2.

(G) Summary bar graph showing GIRK current amplitudes with and without GRK2 co-expression. Unpaired t-tests compared to mGluR3 control, ** p=0.002 for 1x GRK2, *** p<0.0001 for 2x GRK2.

(H) Scatter plot showing the relationship between desensitization kinetics and current amplitude of mGluR3-mediated GIRK currents, with and without 2x overexpression of GRK2.

(I) Quantification of the fluorescence of GFP-tagged WT GRK2 and mutants expressed in cells. The number of fields of cells analyzed are in parentheses. Unpaired t-test, *** p<0.0001.

(J) Representative whole cell patch clamp recordings of GIRK currents mediated by mGluR3 activation with and without overexpression of either GRK2-K220R or GRK2-R587Q.

(K) Summary bar graph of the percent desensitization of mGluR2 or mGluR3-mediated GIRK currents during 30 s glutamate application, with and without overexpression of WT or mutant GRK2, or β-arrestin1 and β-arrestin2. Unpaired t-tests compared to mGluR3 control, * p=0.04 for 1xGRK2, *** p<0.0001 for 2xGRK2.

(L) Quantification of the tau of desensitization of mGluR8-mediated GIRK currents over 30 s 100 μM glutamate application, without (control) and with GRK2 overexpression. Unpaired t-test, ** p=0.009.

(M and N) Representative whole cell patch clamp recordings of GIRK currents mediated by mGluR7 (M) and mGluR4 (N), without (control) and with GRK2 overexpression.

(O) Summary scatter bar graph of the percent desensitization of group III mGluR-mediated GIRK currents over 30 s 100 uM glutamate application for mGluR4 and mGluR8, and 40 s 1-10 mM glutamate application for mGluR7. Unpaired t-test, * p=0.03.

(P) Summary scatter bar graph of the peak GIRK current amplitudes following activation of group III mGluRs. mGluR4 and mGluR8 were activated with 100 uM glutamate while mGluR7 was activated with either 1 mM or 10 mM glutamate. Unpaired t-tests, * p=0.02 for mGluR4, *** p<0.0001 for mGluR8, * p=0.04 for mGluR8.

(Q) Representative average traces of the first calcium transient mediated by activation of mGluR5 without (control) and with GRK2 overexpression.

(R) Average fluorescence intensities of the peak calcium transient mediated by activation of either mGluR1 or mGluR5, without (control) or with overexpression of GRK2 or GRK2-K220R. In parentheses is the number of experiments analyzed per condition.

(S) Quantification of the tau of desensitization from the peak to the end of the first calcium transient mediated by activation of mGluR1 or mGluR5, without (control) or with overexpression of either GRK2 or GRK2-K220R. Unpaired t-tests, p=0.006 for mGluR1 control vs GRK2, p=0.004 for control vs K220R; p=0.05 for mGluR5 control vs GRK2, p=0.05 for control vs K220R. In parentheses is the number of experiments analyzed per condition.

(T) Representative calcium transients mediated by the activation of mGluR5, without (control) or with overexpression of GRK2.

(U) Summary bar graph of the percentage of cells that exhibit calcium oscillations following activation of mGluR5 without (control) or with overexpression of either GRK2 or GRK2-K220R. Unpaired t-tests, ** p=0.008 for control vs GRK2; ** p=0.005 for control vs K220R. In parentheses is the number of experiments analyzed per condition.
In parentheses is the number of individual cells that measurements were taken from, unless otherwise stated. Error bars show s.e.m.

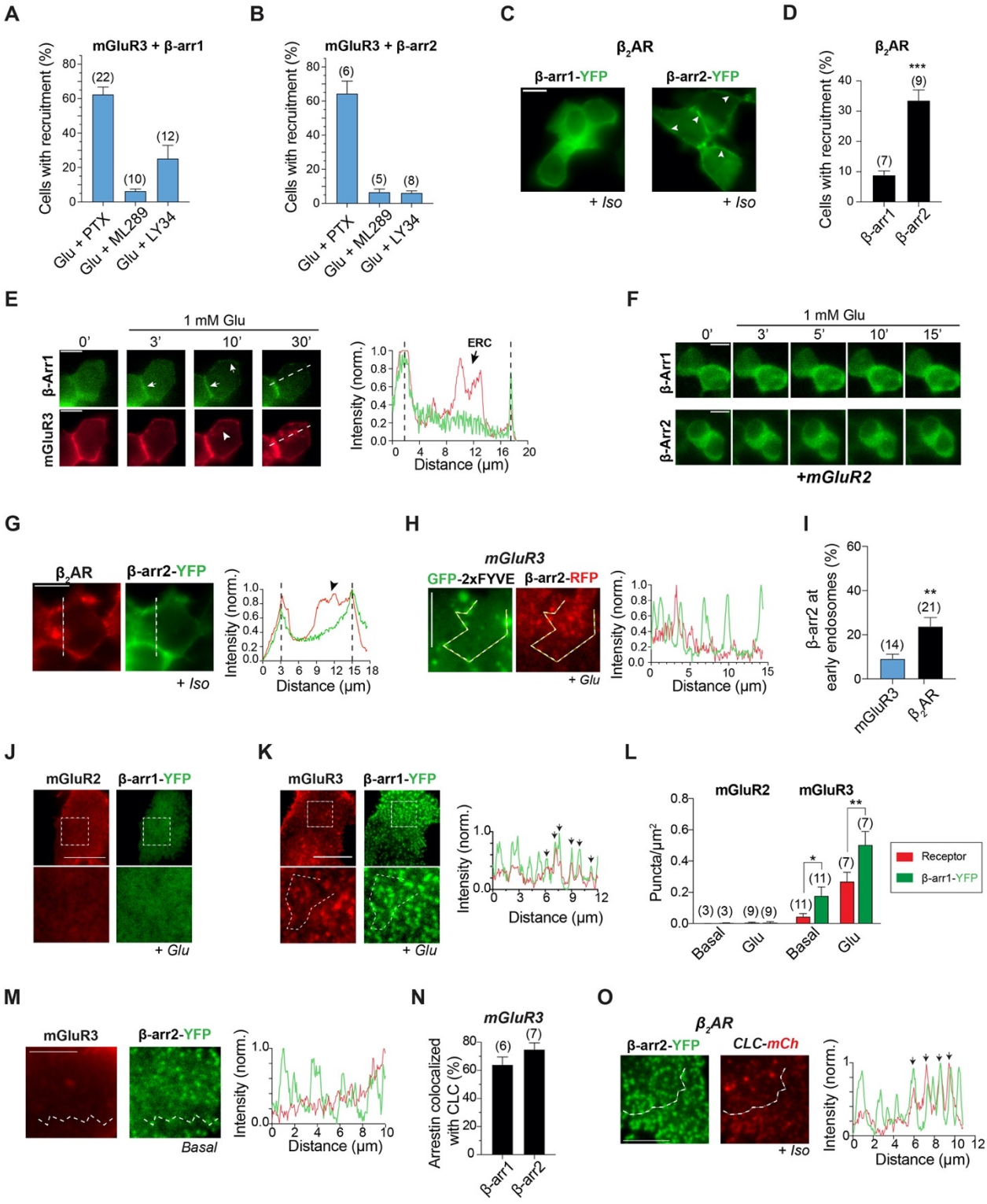

Figure S5. Further analysis of arrestin coupling to mGluR3, Related to Figure 4

(A-B) Summary bar graphs of the percentage of mGluR3-expressing HEK 293T cells that exhibit surface recruitment of β-arr1 (A) or β-arr2 (B) following 15 min glutamate treatment and either co-expression of PTX, treatment with 100 μM ML289, or 20 μM LY34. Number of fields of cells analyzed are shown in parentheses.

(C) Representative images of cells expressing β-arr1-YFP or β-arr2-YFP with β_2AR following 15 min in 10 μM Iso. White arrowheads point at β-arr2-YFP on the cell surface. Scale bar= 10 μm.
(D) Quantification of the percentage of cells that exhibit surface recruitment of β-arr1 or β-arr2 following activation of β_2AR with isoproterenol. Experiment was conducted 48 hr post-transfection. Unpaired t-test, *** $p<0.0001$. Number of fields of cells analyzed are in parentheses.
(E) Left, time-lapse images of a HEK 293T cell expressing BG-546-labeled mGluR3 and β-arr1-YFP. Following treatment with glutamate, surface recruitment of β-arr1 is observed within 3 min and remains on the surface for 30 min. Colocalization between β-arr1-YFP and internalized mGluR3 is not observed at 30 min. White arrows point at β-arr1-YFP on the cell surface. White arrowhead marks internalized mGluR3. Right, intensity line scan along the white dotted line on the 30' images, showing that β-arr1 (green line) and mGluR3 (red line) are present at the cell surface (black dotted lines), but β-arr1 does not accumulate at the ERC with mGluR3.
(F) Time-lapse images showing the lack of β-arr1 and β-arr2 surface recruitment following activation of mGluR2 with glutamate.
(G) Left, representative image of a cell expressing BG-546-labeled β_2AR and β-arr2-YFP, following incubation in isoproterenol for 20 min. β_2AR shows internalization while β-arr2-YFP remains on the surface and does not co-internalize. Right, line scan along the dotted white lines on the images showing the intensity profiles of β-arr1 (green line) and β_2AR (red line). Black dotted lines present the cell surface. The black arrowhead points to internalized β_2AR.
(H) Left, TIRF images showing GFP-2xFYVE-positive early endosomes and β-arr2-RFP puncta following activation of mGluR3 with 1 mM glutamate for 15 min. Right, intensity line scan through the white dotted lines in the images, showing that 2xFYVE peaks (green) do not contain β-arr2 peaks (red).
(I) Quantification of the percentage of β-arr2 puncta that colocalize with GFP-2xFYVE puncta following 15 min activation of either mGluR3 or β_2AR. Unpaired t-test, ** $p=0.008$. Number of cells analyzed are in parentheses.
(J and K) Representative TIRF images of HEK 293T cells expressing β-arr1-YFP and either BG-546-labeled mGluR2 (J) or mGluR3 (K). Activation of mGluR2 with glutamate for 15 min does not generate β-arr1 puncta (J), but mGluR3 activation leads to the formation of both mGluR3 and β-arr1 puncta (K). Intensity line scan through the white dotted line reveals some co-localizing mGluR3 (red line) and β-arr1 (green line) puncta as indicated by the black arrows. Scale bar= 10 μm.
(L) Quantification of the density of receptor (red bars) and β-arr1 (green bars) puncta under basal and glutamate conditions. Number of cells analyzed are in parentheses. Paired t-tests, * $p=0.03$ for mGluR3 basal, ** $p= 0.008$ for mGluR3 + Glu.
(M) Left, TIRF image showing negligible mGluR3 puncta and clear β-arr2 puncta generated under basal conditions. Bottom, intensity line scan through the white dotted line on the image, showing background mGluR3 fluorescence (red line) and clear β-arr1 peaks (green line).
(N) Quantification of the percentage of β-arr-YFP puncta that colocalize with CLC-mCherry puncta following activation of mGluR3 with glutamate for 15 min. Number of cells analyzed are in parentheses.
(O) Left, representative TIRF images of cells expressing β-arr2-YFP and CLC-mCherry with co-expression of β_2AR. Right, Line scan through the white dotted lines on the images show β-arr2 peaks (green line) and CLC peaks (red line). The black arrows denote overlapping peaks.
Scale bar= 10 μm in C, E, F, G, J, K; 5 μm in H, M, N. Error bars show s.e.m.

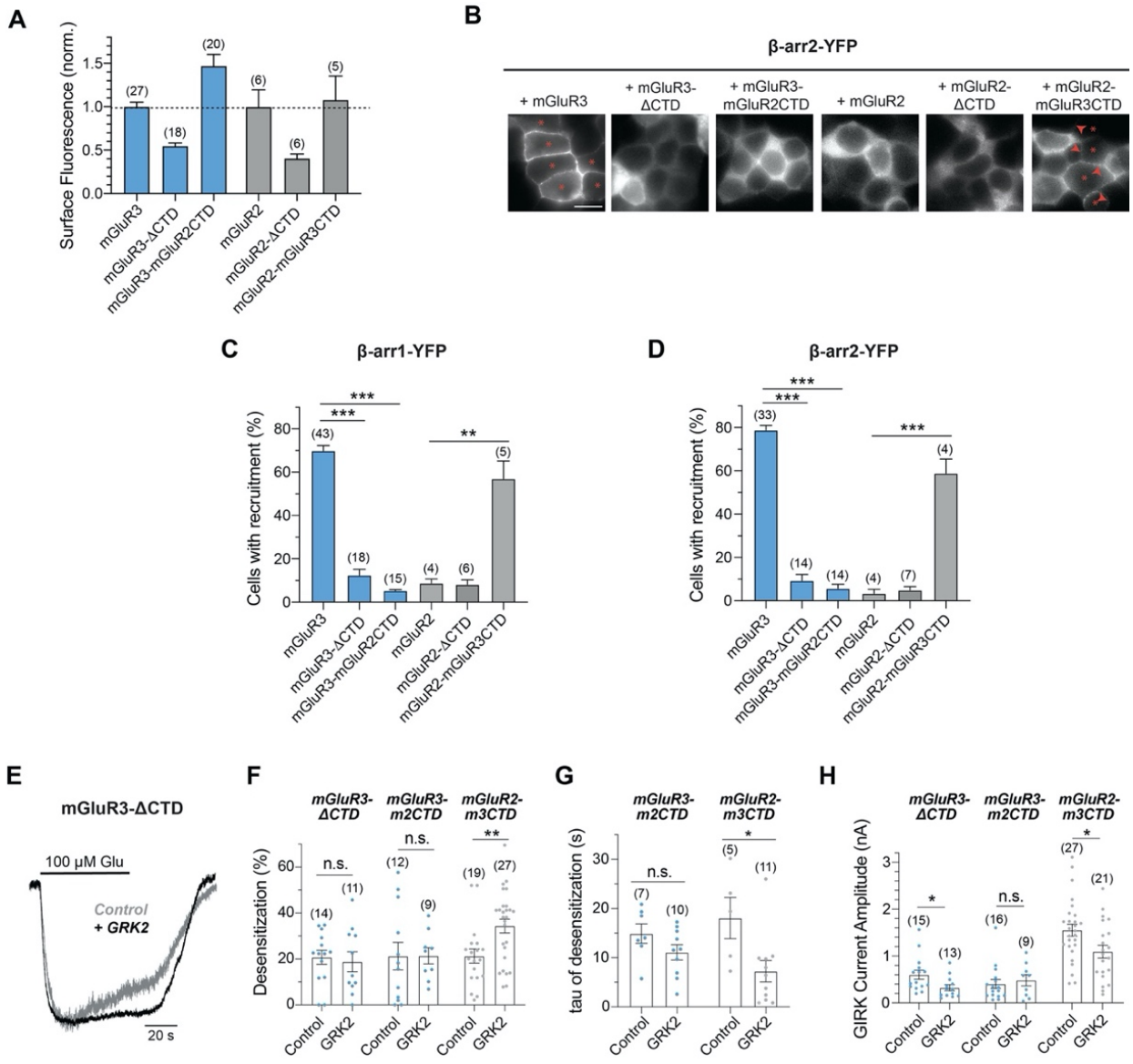

Figure S6. Further characterization of the C-terminal domains of mGluR2 and mGluR3, Related to Figure 5

(A) Surface fluorescence of BG-546-labeled SNAP-tagged CTD constructs in HEK 293T cells. Fluorescence was measured after 24 hr expression for mGluR3 variants, and at 48 hr expression for mGluR2 variants. All values were normalized to the average fluorescence of mGluR3. In parentheses is the number of fields of cells that were analyzed.

(B) Representative images of HEK 293T cells expressing β-arr2-YFP following activation of either mGluR3 or mGluR2 CTD variants with 15 min glutamate. Red asterisks mark cells that exhibit surface recruitment of β-arr2. Red arrowheads point at regions on the cell surface with β-arr2 recruitment. Scale bar=10 μm.

(C and D) Summary bar graphs with quantification of the percentage of cells that exhibit β-arr1 (C) or β-arr2 (D) surface recruitment following glutamate application. In parentheses is the number of fields of cells that were analyzed. Unpaired t-tests, *** $p<0.0001$ for β-arr1 mGluR3 vs mGluR3-ΔCTD, *** $p<0.0001$ for β-arr1 mGluR3 vs mGluR3-mGluR2CTD, ** $p= 0.002$ for β-arr1 mGluR2 vs mGluR2-mGluR3CTD,

*** p<0.0001 for β-arr2 mGluR3 vs mGluR3-ΔCTD, *** p<0.0001 for β-arr2 mGluR3 vs mGluR3-mGluR2CTD, *** p=0.0002 for β-arr2 mGluR2 vs mGluR2-mGluR3CTD.
(E) Representative whole cell patch clamp recordings of GIRK currents mediated by the activation of mGluR3-ΔCTD with and without GRK2 overexpression in HEK 293T cells.
(F) Summary scatter bar graph of the percent desensitization of GIRK currents during activation of the CTD variants with glutamate. Desensitization was measured over 60 s for mGluR3-ΔCTD and over 30 s for mGluR3-mGluR2CTD and mGluR2-mGluR3CTD. Unpaired t-test, ** p=0.005. The number of cells recorded from are in parentheses.
(G) Summary scatter bar graph of the tau of desensitization of GIRK currents over ~30 s glutamate application to activate mGluR3-mGluR2CTD or mGluR2-mGluR3CTD without (control) or with GRK2 overexpression. Unpaired t-test, * p=0.02. The number of cells recorded from are in parentheses.
(H) Summary scatter bar graph of GIRK current amplitudes following activation of the CTD variants, with and without co-expression of GRK2. Unpaired t-tests, * p=0.03 for mGluR3-ΔCTD, * p=0.02 for mGluR2-mGluR3CTD. The number of cells recorded from are in parentheses.
Error bars show s.e.m.

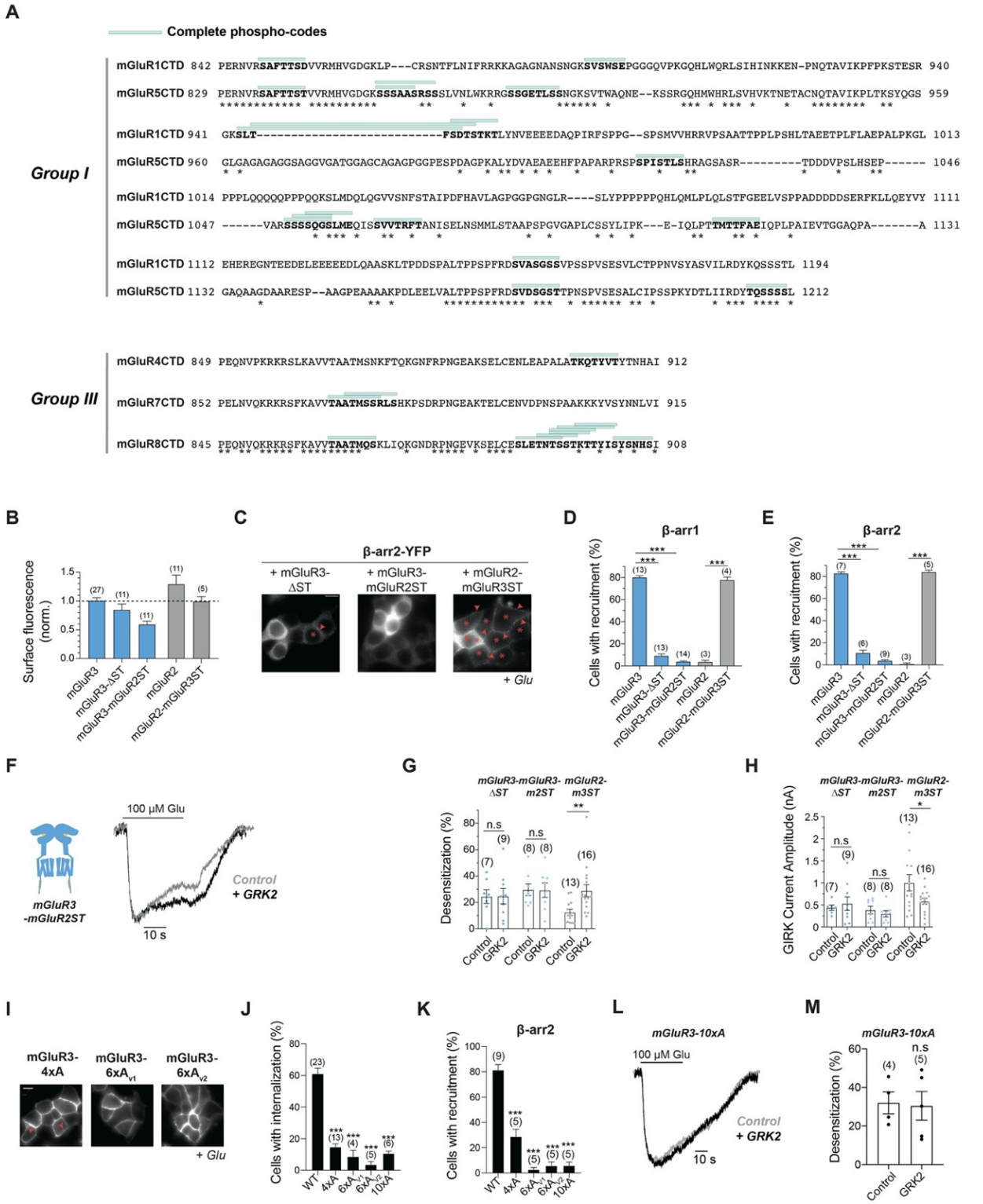

Figure S7. Further analysis of ST-rich sequences and their role in desensitization, Related to Figure 6

(A) The C-terminal domain sequences of group I and group III mGluRs. * indicates residues that are the same between sequences of the same group. Predicted complete phospho-codes are highlighted along the sequences as determined by PhosCoFinder (*Zhou et al., Cell, 2017*).

(B) Quantification of the surface fluorescence of BG-546-labeled SNAP-tagged ST variants in HEK 293T cells. Fluorescence was measured after 24 hr expression for mGluR3 variants, and at 48 hr expression for mGluR2 variants. All values were normalized to the average fluorescence of mGluR3. In parentheses is the number of fields of cells that were analyzed.
(C) Representative images of HEK 293T cells expressing β-arr2-YFP following activation of either ST variants with glutamate for 15 min. Red asterisks mark cells that exhibit surface recruitment of β-arr2. Red arrowheads point at regions on the cell surface with β-arr2 recruitment.
(D and E) Summary bar graphs with quantification of the percentage of cells that exhibit β-arr1 (D) or β-arr2 (E) surface recruitment following glutamate application. In parentheses is the number of fields of cells that were analyzed. Unpaired t-tests, *** $p<0.0001$ for all comparisons shown.
(F) Representative whole cell patch clamp recording of GIRK currents mediated by the activation of mGluR3-mGluR2ST with and without GRK2 overexpression in HEK 293T cells.
(G and H) Summary scatter bar graphs of the percent desensitization (G) and peak amplitudes (H) of GIRK currents mediated by ST variants, without (control) and with GRK2 overexpression. Desensitization was measured over 30 s glutamate application. Unpaired t-tests, ** $p=0.006$ for percent desensitization, * $p=0.03$ for amplitudes. The number of cells recorded from are in parentheses.
(I) Representative images of HEK 293T cells expressing mGluR3 alanine mutants. Cells were treated with 1 mM Glu for 30 min. Red arrows point at internalized receptors.
(J and K) Summary bar graphs showing the percentage of cells that exhibit internalization (J) or surface recruitment of β-arr2 (K) across mGluR3 alanine mutants.
(L) Representative whole cell patch clamp recording of GIRK currents mediated by activation of mGluR3-10xA without (control) and with GRK2 overexpression.
(M) Quantification of the percent desensitization of mGluR3-10xA-mediated GIRK currents over 30 s of glutamate application, without (control) and with GRK2 overexpression. The number of cells recorded from are in parentheses.
Scale bars= 10 μm. Error bars show s.e.m.

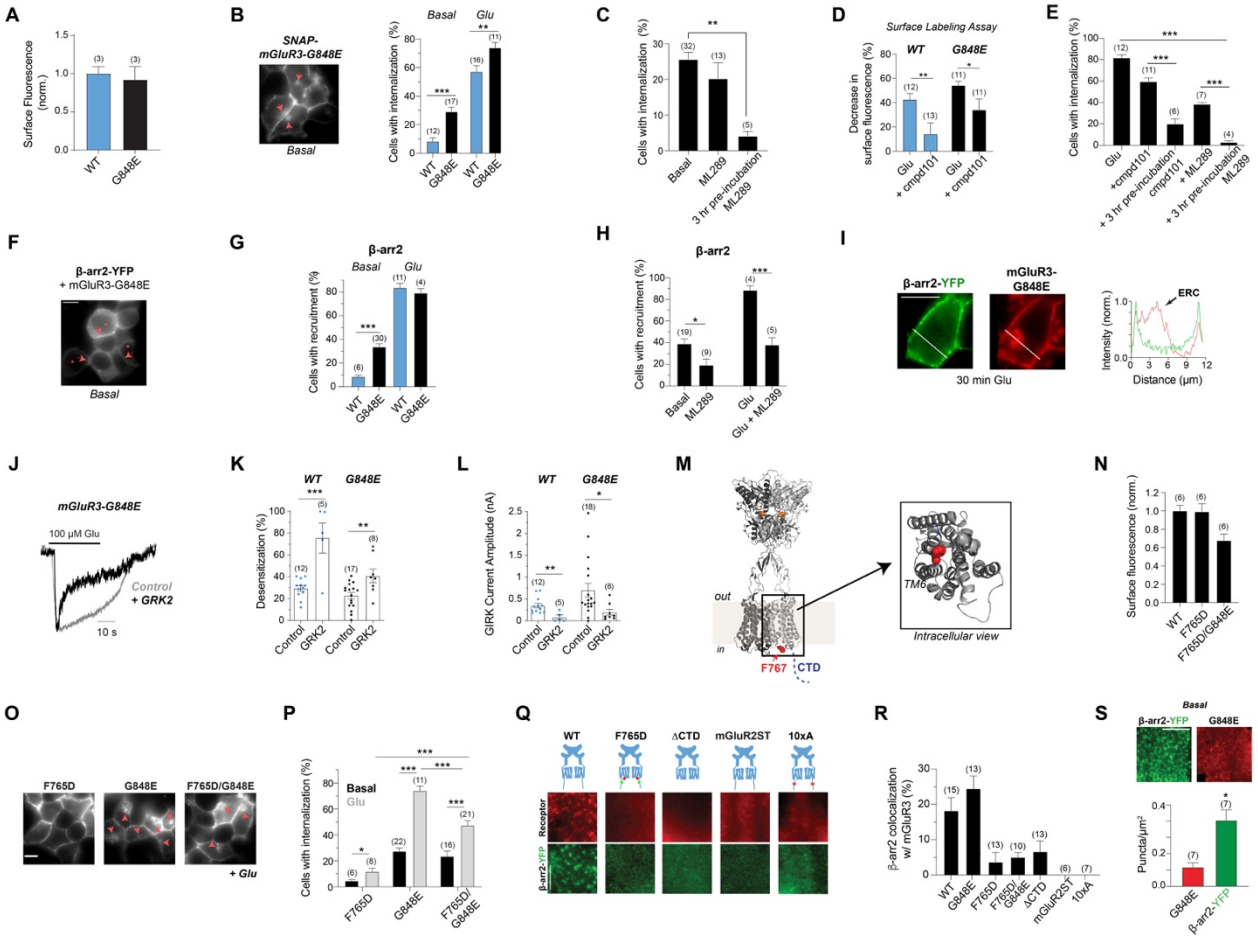

Figure S8. Further analysis of the role of the transmembrane core and CTD in β-arrestin coupling to mGluR3, Related to Figure 7

(A) Quantification of the surface fluorescence of BG-546-labeled SNAP-mGluR3 WT and G848E in HEK 293T cells. The number of independent experiments is shown in parentheses.

(B) Left, representative images of cells showing basal internalization of BG-546-labeled mGluR3-G848E. Red arrows point to internalized receptors. Scale bar= 10 μm. Right, Quantification of the percentage of cells that show internalization of mGluR3 WT or G848E under basal conditions and after 30 min glutamate treatment. Unpaired t-tests, *** p<0.0001 for basal, ** p=0.008 for Glu. The number of fields of cells analyzed is shown in parentheses.

(C) Summary bar graph of the percentage of cells that exhibit basal internalization of mGluR3-G848E following preincubation in ML289. The number of fields of cells analyzed is in parentheses. Unpaired t-test, *** p<0.0001.

(D) Quantification of the percent surface fluorescence decrease as measured using the surface labeling assay. The number of fields of cells analyzed is in parentheses. Unpaired t-tests, ** p=0.009 for WT and * 0.05 for G848E).

(E) Quantification of the percentage of cells that exhibit internalization following 30 min treatment with Glu with either cmpd101 or ML289. Pre-incubation refers to the amount of time cells were incubating in cmpd101 or ML289 prior to Glu treatment. The number of fields of cells analyzed is in parentheses. Unpaired t-tests, *** p<0.0001 for all comparisons made.

(F) Representative image showing surface recruitment of β-arr2-YFP by mGluR3-G848E under basal conditions. Red asterisks denote the cells that show β-arr2 recruitment, the red arrows point to regions on the cell surface with β-arr2. Scale bar=10 μm.

(G) Quantification of the percentage of cells that exhibit β-arr2 recruitment by mGluR3 WT and G848E under basal conditions and after 15 min glutamate. Unpaired t-test, *** p=0.0004. The number of fields of cells analyzed is shown in parentheses.
(H) Quantification of the percentage of cells that show β-arr2 surface recruitment of mGluR3-G848E following 15 min incubation in the indicated drugs. The number of fields of cells analyzed is in parentheses. Unpaired t-tests, * p=0.02 for basal vs ML289, *** p=0.0007 for Glu vs Glu + ML289.
(I) Left, representative images of a cell showing β-arr2-YFP on the cell surface and internalized receptor in the ERC following incubation in glutamate. Right, intensity line scan along the white line on the images, showing the overlap of β-arr2-YFP (green line) and receptor (red) at the cell membrane, but not in the ERC. Scale bar= 10 μm.
(J) Representative whole cell patch clamp recordings of GIRK currents mediated by activation of mGluR3-G848E without (control) and with GRK2 overexpression.
(K) Summary scatter bar graph showing the percent desensitization of mGluR3 WT or G848E evoked GIRK currents, with and without GRK2 overexpression, during 30 s glutamate applications. Unpaired t-tests, *** p=0.0009 for WT, ** p= 0.003 for G848E). The number of cells recorded from are in parentheses.
(L) Summary scatter bar graph showing the peak amplitudes of GIRK currents mediated by mGluR3-G848E activation, without (control) and with GRK2 overexpression. Unpaired t-tests, ** p=0.009 for WT, * p=0.03 for G848E. The number of cells recorded from are in parentheses.
(M) Structural model of ligand-bound (orange) mGluR5, showing the location of the conserved residue, F767 (red), and the CTD (blue).
(N) Quantification of the surface fluorescence BG-546-labeled mGluR3 WT, F765D, and F765D/G848E in HEK 293T cells. Values were normalized to the average surface fluorescence of mGluR3 WT. The number of fields of cells analyzed is in parentheses.
(O) Representative images of cells expressing mGluR3-F765D, G848E, or F765D/G848E, following incubation in glutamate for 30 min. Red arrows point at internalized receptors. Scale bar= 10 μm.
(P) Quantification of the percentage of cells that exhibit internalization of mGluR3 mutants under basal and glutamate conditions. The number of fields of cells analyzed is in parentheses. Unpaired t-tests, * p=0.04 for F765D, *** p<0.0001 for G848E, *** p=0.0001 for F765D/G848E, *** p<0.0001 for G848E vs F765D/G848E, *** p<0.0001 for F765D vs F765D/G848E.
(Q) Representative TIRF images of β-arr2-YFP and mGluR3 variants following glutamate treatment for 15 min. Scale bar= 5 μm.
(R) Summary bar graph of the percent colocalization of β-arr2 puncta with the puncta of mGluR3 variants. The number of cells analyzed are shown in parentheses.
(S) Top, TIRF image showing β-arr2-YFP puncta under basal conditions with co-expression mGluR3-G848E. Bottom, quantification of the density of mGluR3-G848E puncta and β-arr2-YFP puncta under basal conditions. The number of cells analyzed are in parentheses. Paired t-test, * p=0.01. Scale bar= 5 μm.
Error bars show s.e.m.